Article

# Dietary fructose improves intestinal cell survival and nutrient absorption

https://doi.org/10.1038/s41586-021-03827-2

Received: 14 April 2020

Accepted: 15 July 2021

Published online: 18 August 2021

Check for updates

Samuel R. Taylor[1,2,3,4], Shakti Ramsamooj[1,2], Roger J. Liang[1,2], Alyna Katti[2,4], Rita Pozovskiy[1,2], Neil Vasan[2,5], Seo-Kyoung Hwang[1,2], Navid Nahiyaan[6], Nancy J. Francoeur[7], Emma M. Schatoff[1,2,3], Jared L. Johnson[2], Manish A. Shah[2], Andrew J. Dannenberg[2], Robert P. Sebra[7,8], Lukas E. Dow[2], Lewis C. Cantley[2], Kyu Y. Rhee[6] & Marcus D. Goncalves[1,2]✉

Fructose consumption is linked to the rising incidence of obesity and cancer, which are two of the leading causes of morbidity and mortality globally[1,2]. Dietary fructose metabolism begins at the epithelium of the small intestine, where fructose is transported by glucose transporter type 5 (GLUT5; encoded by *SLC2A5*) and phosphorylated by ketohexokinase to form fructose 1-phosphate, which accumulates to high levels in the cell[3,4]. Although this pathway has been implicated in obesity and tumour promotion, the exact mechanism that drives these pathologies in the intestine remains unclear. Here we show that dietary fructose improves the survival of intestinal cells and increases intestinal villus length in several mouse models. The increase in villus length expands the surface area of the gut and increases nutrient absorption and adiposity in mice that are fed a high-fat diet. In hypoxic intestinal cells, fructose 1-phosphate inhibits the M2 isoform of pyruvate kinase to promote cell survival[5–7]. Genetic ablation of ketohexokinase or stimulation of pyruvate kinase prevents villus elongation and abolishes the nutrient absorption and tumour growth that are induced by feeding mice with high-fructose corn syrup. The ability of fructose to promote cell survival through an allosteric metabolite thus provides additional insights into the excess adiposity generated by a Western diet, and a compelling explanation for the promotion of tumour growth by high-fructose corn syrup.

Humans in the Western world consume more fructose now than ever before in recorded history. Agricultural and industrial advances have improved the access to sweeteners like sucrose and high-fructose corn syrup (HFCS), which have tripled the total consumption of fructose and contributed to a burgeoning epidemic of obesity and related diseases[8,9]. The global rise in obesity is directly linked to an increase in obesity-related cancers such as colorectal cancer (CRC), the incidence and mortality of which are rising among young adults[10,11]. Several observations suggest that there is a causal relationship between fructose consumption and CRC. For example, fructose consumption is associated with the incidence and progression of gastrointestinal cancer[2,12–14], and drives tumour growth and metastasis in mouse models of CRC[15,16].

As tumour growth is driven by hyperplasia and tumour cells frequently retain metabolic pathways from their tissue of origin, we hypothesized that fructose would promote hyperplasia of the normal intestinal epithelium just as it promotes growth in intestinal tumours. To assess this, we fed mice HFCS for four weeks and quantified the mean intestinal villus length using a high-throughput, unbiased image-segmentation-based approach (Extended Data Fig. 1a–f). Mice of both sexes and a variety of ages and genetic backgrounds that were treated with HFCS showed a 25–40% increase in intestinal villus length in the duodenum and proximal jejunum compared to $H_2O$-treated control mice (Fig. 1a, Extended Data Fig. 1h). The increase in villus length correlated with increased weight gain and fat accumulation as well as lipid absorption (Extended Data Fig. 2a–l).

We hypothesized that this increase in absorption would exacerbate weight gain in mice placed on a high-fat diet (HFD) that contained fructose. Over four weeks, mice were treated with a control diet that contained no fructose, a standard HFD (45% of calories from fat) that contained dextrose but no fructose, or an isocaloric HFD in which the dextrose was replaced by sucrose (Supplementary Table 1). Mice on the sucrose-fortified HFD gained significantly more weight and fat mass than those on the standard HFD, despite consuming and expending the same amount of energy (Fig. 1b, c, Extended Data Fig. 2m–v). In agreement with the data from mice that consumed a normal chow (low-fat) diet, mice that were fed fructose in the form of sucrose had a similar small intestinal length but longer villi (Fig. 1d, Extended Data Fig. 2r), exhibited increased levels of serum triglycerides after an oral lipid bolus (Fig. 1e) and lost less energy in the faeces compared to isocaloric, sucrose-free control mice (Extended Data Fig. 2w–z). These data suggest that dietary fructose increases intestinal villus length and nutrient absorption.

[1]Division of Endocrinology, Weill Department of Medicine, Weill Cornell Medicine, New York, NY, USA. [2]Meyer Cancer Center, Weill Department of Medicine, Weill Cornell Medicine, New York, NY, USA. [3]Weill Cornell–Rockefeller–Sloan Kettering Tri-Institutional MD–PhD program, New York, NY, USA. [4]Weill Cornell Graduate School of Medical Sciences, Weill Cornell Medicine, New York, NY, USA. [5]Breast Medicine Service, Memorial Sloan Kettering Cancer Center, New York, NY, USA. [6]Division of Infectious Diseases, Weill Department of Medicine, Weill Cornell Medicine, New York, NY, USA. [7]Department of Genetics and Genomic Sciences, Icahn School of Medicine at Mount Sinai, New York, NY, USA. [8]Sema4, Stamford, CT, USA. ✉e-mail: mdg9010@med.cornell.edu

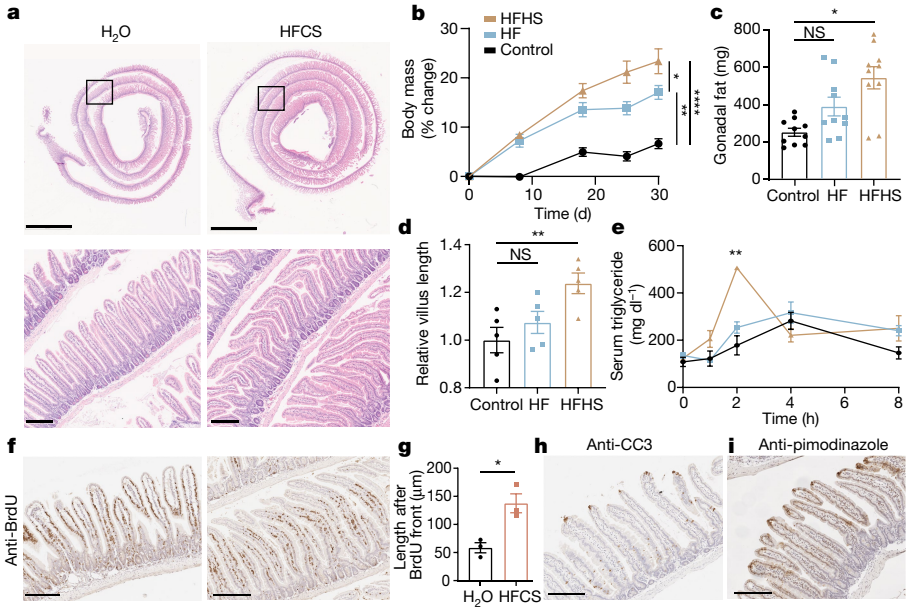


**Fig. 1 | Dietary fructose increases intestinal villus length and lipid absorption. a**, Haematoxylin and eosin (H&E)-stained duodenum from mice that were fed normal chow with ad libitum $H_2O$ or 25% HFCS for four weeks. Scale bars, 3 mm (top); 200 μm (bottom). **b**, Relative change in the body mass of mice that were fed a control diet, a high-fat diet (45% kcal fat) (HF) or a high-fat, high-sucrose diet (HFHS) ($n = 5$ mice per group). **c**, Mass of white adipose tissue from the gonadal depot after five weeks on each diet ($n = 5$ mice per group; two depots per mouse). **d**, Relative duodenal villus length after five weeks on each diet ($n = 5$ mice per group). **e**, Serum triglyceride levels in fasted mice after an oral gavage with olive oil ($n = 3$ mice per group). **f**, BrdU immunohistochemistry (IHC) of duodenal sections from $H_2O$ or HFCS-treated mice 72 h after intraperitoneal BrdU injection. Scale bars, 200 μm. **g**, Duodenal villus length distal to the BrdU front ($n = 3$ mice per group; 40 villi per mouse). **h**, **i**, IHC for CC3 (**h**) and pimodinazole (**i**) in duodenal sections from $H_2O$-treated mice. Scale bars, 200 μm. **b**–**e**, One-way ANOVA followed by Holm–Sidak post-hoc test for multiple comparisons; **g**, two-sided Student's *t*-test. NS, not significant; $^*P < 0.05$, $^{**}P < 0.01$, $^{****}P < 0.0001$; exact *P* values are provided in the Source Data for all figures. All data are mean ± s.e.m.

Intestinal villus length is determined by a balance between the rates of proliferation and death of epithelial cells. Thus, the villus is constantly in a state of self-renewal as stem cells in the crypt divide to yield new intestinal epithelial cells (IECs), which then transit outward until they reach the villus apex and are extruded into the intestinal lumen[17]. To determine whether the longer villi resulted from an increased rate of migration (that is, proliferation) or increased cell survival, we conducted single- and dual-label tracing experiments using 5-bromo-2′-deoxyuridine (BrdU) and 5-ethynyl-2′-deoxyuridine (EdU) injections at several different time points. These assays showed that the duodenal villi of HFCS-treated mice had similar migration rates to those of $H_2O$-treated control mice (Extended Data Fig. 3a-e), but that they had more than twice as many IECs surviving longer than 72 h than did control mice (Fig. 1f, g). There was also no change in cell proliferation as assessed by histologic Ki-67 staining (Extended Data Fig. 3f). These data indicate that cell survival is a major determinant of the hypertrophy of villi in the presence of fructose.

Cell transit up the intestinal villus terminates with cell death and extrusion into the intestinal lumen[17]. Indeed, in all cases in which extruding cells were captured in histological sections, staining for the apoptosis marker cleaved caspase-3 (CC3) or for terminal deoxynucleotidyl transferase dUTP nick-end labelling (TUNEL) was positive, regardless of diet (Fig. 1h, Extended Data Fig. 3f). Because IECs migrate away from their blood supply during their transit along the villus, this cell death is likely to be influenced by tissue hypoxia. Consistent with this theory, pimonidazole staining, which is used to indicate tissues in which the partial pressure of oxygen is less than 10 mm Hg, correlated with distance from the muscularis layer in the small and large intestine of both $H_2O$-treated and HFCS-treated mice (Fig. 1i, Extended Data Fig. 3g, h). Despite this apparent similarity in hypoxia patterns between $H_2O$- and HFCS-treated mice, we observed an increase in the hypoxia-inducible factor-1α (HIF-1α) target proteins enolase-1 (ENO1) and lactate dehydrogenase A (LDHA) in the intestinal epithelium of HFCS-treated mice, and a strong upregulation of the fructolytic proteins GLUT5 and ketohexokinase (KHK) (Extended Data Fig. 3i–k).

As hypoxia is a driver of cell death in a wide variety of tissues and contexts, we next examined whether fructose could also mitigate cell death in human CRC cell lines cultured in hypoxia. The addition of fructose did not affect the cell growth rate but did improve the survival of hypoxic HCT116 and DLD1 cells (Fig. 2a, b, Extended Data Fig. 4a–f). Fructose also improved the survival of hypoxic mouse intestinal organoids. Hypoxia induced intense apoptosis in the organoid core (the morphological correspondent to the villus), which was reflected by both increased CC3 intensity and a decreased population of viable cells, and these changes were abrogated by treatment with fructose (Extended Data Fig. 4g, h). We observed no increase in organoid proliferation with fructose treatment (Extended Data Fig. 4i), indicating that the benefit of fructose is primarily attributable to cell survival in this context as well.

Fructose is mainly transported into intestinal cells by the sugar transporter GLUT5, before it is phosphorylated by KHK to form fructose 1-phosphate (F1P). In human CRC cells, the total levels of KHK were consistent regardless of fructose or hypoxia exposure, whereas hypoxia induced an increase in the abundance of GLUT5 (Extended Data Fig. 5a). Notably, treatment with cobalt chloride led to robust stabilization of HIF-1α, but did not induce the upregulation of GLUT5, suggesting that GLUT5 expression is independent of HIF-1α protein levels. We also noted strong expression of KHK-A in hypoxia in human CRC cells (Extended Data Fig. 5b, c) and confirmed that exogenous fructose was converted to F1P, but that fructose carbon atoms were not incorporated into downstream glycolytic intermediates (Fig. 2c, Extended Data Fig. 6a), consistent with previous studies in mouse intestinal tumours[15]. This agreed with our observation that fructose was

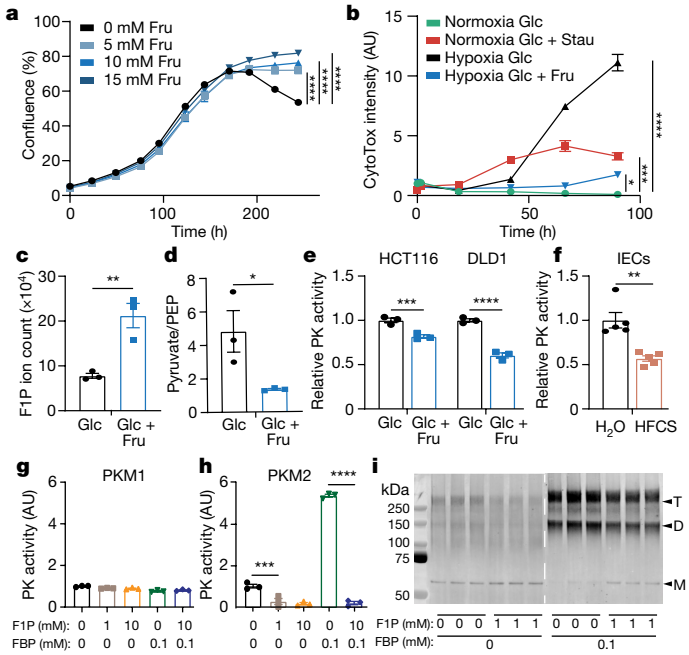


**Fig. 2 | Fructose metabolism enhances hypoxic cell survival and decreases pyruvate kinase activity. a**, Confluence of HCT116 cells grown in hypoxia with varying concentrations of fructose (Fru) ($n = 3$ biological replicates per group). **b**, CytoTox viability dye intensity in HCT116 cells cultured in glucose medium with and without fructose. Stain intensity is reported as positive area per well normalized to the initial normoxic glucose control ($n = 3$ biological replicates per group). Glc, glucose; Stau, stausporin control. AU, arbitrary units. In these and other cell viability assays, unless otherwise noted, glucose was replenished daily (see Methods). **c**, **d**, Quantification of metabolites (F1P ion count (**c**); pyruvate to PEP ratio (**d**)) in hypoxic HCT116 cells, via liquid chromatography–mass spectrometry (LC–MS) ($n = 3$ biological replicates per group). **e**, **f**, Pyruvate kinase (PK) activity in hypoxic HCT116 and DLD1 cell lysates and in IEC lysates from mice that were fed the indicated diets (glucose or glucose plus fructose (**e**); $H_2O$ or HFCS (**f**)) for four weeks ($n = 3$ independent reaction wells per group; same final protein concentration in each well). **g**, **h**, Pyruvate kinase activity of recombinant pyruvate kinase isozymes (PKM1 (**g**); PKM2 (**h**)) that were pre-incubated with the indicated metabolites ($n = 3$ wells per group). **i**, Western blot against PKM2 using recombinant PKM2 samples cross-linked with disuccinimidyl glutarate ($n = 3$ independent reaction wells per group). T, D and M indicate the putative sizes of tetrameric, dimeric and monomeric PKM2, respectively. **a**, **b**, **g**, **h**, One-way ANOVA followed by Holm–Sidak post-hoc test for multiple comparisons; **c**, **d**, **f**, two-sided Student's *t*-test; **e**, two-way ANOVA followed by Holm–Sidak post-hoc test for multiple comparisons. $^*P < 0.05$, $^{**}P < 0.01$, $^{***}P < 0.001$, $^{****}P < 0.0001$. All data are mean ± s.e.m. For gel source data, see Supplementary Fig. 1.

not depleted from the medium of either human CRC cells or mouse intestinal organoids cultured in hypoxia (Extended Data Fig. 6d–d). In fact, direct fructose metabolites explained only a small portion of the distinct metabolic signature that is associated with fructose exposure in hypoxia (Extended Data Fig. 6e, Supplementary Fig. 3). Upper glycolytic intermediates, however, were increased in hypoxic HCT116 cells and the ratio of pyruvate to phosphoenolpyruvate (PEP) was significantly lower, consistent with inhibition of pyruvate kinase (Fig. 2d, Extended Data Fig. 6f). Pyruvate kinase is the final rate-limiting enzyme in glycolysis that converts pyruvate to PEP, and the activity of the M2 isoform (PKM2) is highly sensitive to changes in the intracellular metabolome[18]. Moreover, PKM2 expression is high in tissues that are subject to hypoxia, such as tumours and intestinal villi[15,19]. Using enzymatic assays, we confirmed the inhibition of pyruvate kinase in CRC cell lysates exposed to fructose and in IEC lysates from mice that were fed with HFCS (Fig. 2e, f, Extended Data Fig. 6g).

Because F1P is structurally similar to the endogenous regulator of PKM2, fructose 1,6-bisphosphate (FBP), we hypothesized that F1P might directly inhibit the activity of PKM2. FBP binds tightly in a regulatory pocket distant from the active site and stabilizes PKM2 in a highly active tetramer. Docking simulations showed that F1P can occupy the same pocket but lacks the outward-facing phosphate group that is necessary to interact with an adjacent peptide loop that is critical for tetramer formation[20] (Extended Data Fig. 7a). Consistent with this mechanism, we found that F1P robustly inhibited PKM2 but did not inhibit PKM1, which lacks the FBP-binding pocket[18] (Fig. 2g, h), and that this inhibition was accompanied by a decrease in the proportion of tetrameric to monomeric enzyme (Fig. 2i, Extended Data Fig. 7b, c). By contrast, PKL—a pyruvate kinase isozyme with a modified type of FBP-binding pocket—was only partially inhibited by F1P (Extended Data Fig. 7d). In an FBP-unresponsive mutant version of PKM2 (PKM2(R489L))[20], we still noted strong inhibition, suggesting that F1P not only competes with FBP for binding but also directly inhibits PKM2 once bound (Extended Data Fig. 7e). In line with this, we found that the interaction between F1P and Ser519—a residue deep in the binding pocket—is critical for inhibition, as mutation of this serine residue to alanine ablated F1P inhibition while preserving FBP activation (Extended Data Fig. 7f–h). The inhibitory effects of F1P could be also be overcome by using the small molecule TEPP-46 to activate PKM2 at a site remote from the FBP pocket[7] (Fig. 3a, Extended Data Fig. 7i).

To test whether PKM2 activity could influence the effects of fructose in cells and tissues, we first generated HCT116 cells in which PKM2 mRNA was knocked down using short hairpin RNA (shRNA), and exposed these cells to hypoxia in the presence or absence of fructose. In the setting of PKM2 depletion, fructose no longer improved hypoxic cell survival (Fig. 3b, Extended Data Fig. 8a). Similarly, when we used TEPP-46 to activate PKM2 in cells, the effects of fructose were greatly diminished (Fig. 3c, Extended Data Fig. 8b). These data suggest that PKM2 is a key mediator of fructose-induced cell survival.

The ability to change activity and conformation in response to stimuli probably explains the high expression of PKM2 in rapidly dividing tissues, which must contend with nutrient and oxygen constraints to continue their growth. In low-oxygen states, for example, the inhibition of PKM2 mitigates reactive oxygen species to improve cell survival[5]. Consistent with this role, we observed that fructose reduced the total amount of $H_2O_2$ in hypoxic cells, an effect that was abrogated by PK activation and was not observed in *PKM2*-knockdown cells (Extended Data Fig. 8c–e). The PKM2 monomer and dimer are also known to bind and transactivate HIF-1α, a key transcription factor for hypoxic adaptation[21]. Because F1P triggers the formation of these lower-order PKM2 units, we hypothesized that fructose would increase HIF-1α transactivation. Indeed, hypoxic and normoxic HCT116 cells exposed to fructose had increased HIF-1α transcriptional activity, and this result was abrogated by two structurally distinct PK activators[21] (Fig. 3d). Moreover, HIF-1α activity correlated with intracellular ATP levels and AMP-activated protein kinase (AMPK) signalling, as well as lactate production in hypoxia (Fig. 3e, Extended Data Fig. 8g–i), consistent with the role of HIF-1α in rewiring cellular metabolism. Together, our data identify F1P as an inhibitor of PKM2, which then amplifies the activity of HIF-1α to promote hypoxic cell survival.

The importance of PKM2 in the physiological response to fructose was confirmed using genetic mouse models. Selective deletion of PKM2 in IECs ($Vil1^{Cre/+}$;$Pkm^{tm1.1Mgvh/tm1.1Mgvh}$ mice; hereafter referred to as $Vil1^{Cre/+}$;$Pkm2^{f/f}$ mice) led to a strong upregulation of PKM1 and increased pyruvate kinase activity in the epithelium (Extended Data Fig. 9a, b), and also altered the nuclear localization of pyruvate kinase (Extended Data Fig. 9c). The villi of these mice, as well as mice lacking KHK ($Khk^{-/-}$ mice), were short and unable to elongate in the presence of HFCS (Fig. 3f), indicating that F1P and PKM2 are both required. Furthermore, the mice deficient in PKM2 or KHK did not upregulate GLUT5 or HIF-1α target proteins (Extended Data Fig. 9d–f) and were

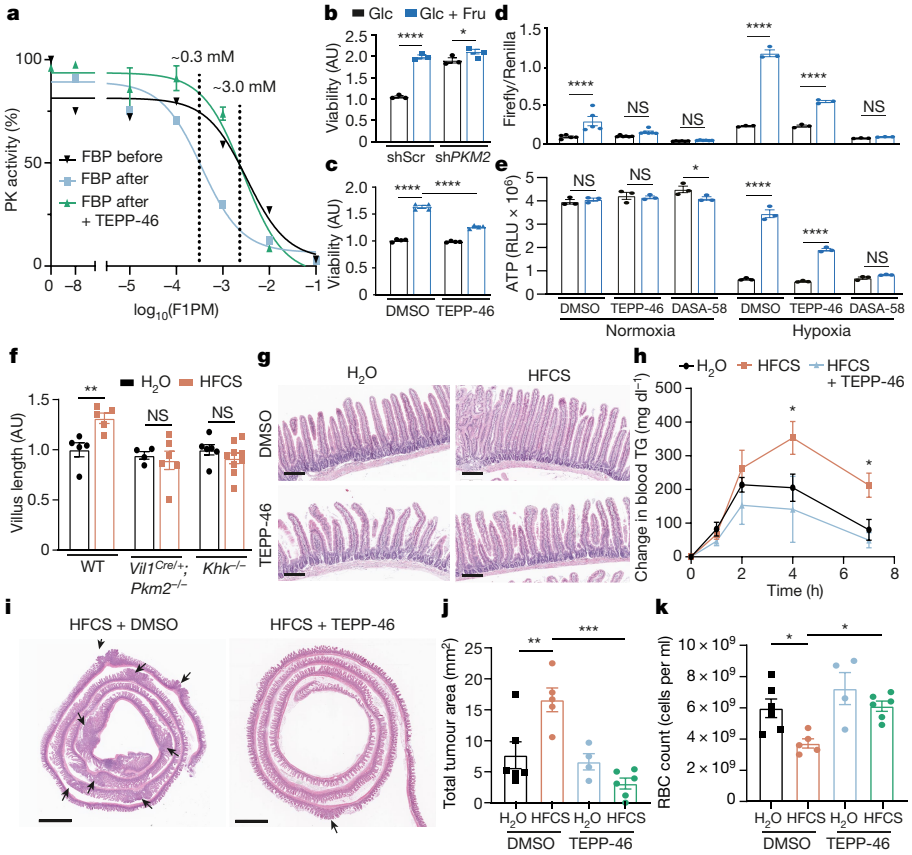


**Fig. 3 | PK activation diminishes the effect of fructose on hypoxia survival.** **a**, PK activity of recombinant PKM2 incubated with varying concentrations of F1P (F1PM indicates the molar concentration of F1P). FBP with or without TEPP-46 was added either before or after F1P. Half-maximal inhibitory concentration ($IC_{50}$) values are as follows. With FBP before F1P incubation: 3.3 mM (95% confidence interval: 1.1–9.6 mM); with FBP after F1P incubation: 0.35 mM (95% CI: 0.15–0.80 mM); with FBP and TEPP-46 after F1P incubation: 2.7 mM (95% CI: 1.7–4.4 mM) ($n = 2$ wells per data point for FBP before; $n = 4$ for FBP after; $n = 3$ for FBP after + TEPP-46). **b**, Viability of HCT116 cells that were virally transduced with the indicated shRNAs (control scrambled shRNA (shScr) or shRNA targeting *PKM2* (sh*PKM2*)) and cultured in hypoxia with or without fructose ($n = 3$ biological replicates per group). **c**, Viability of HCT116 cells that were cultured in hypoxia with or without fructose and with either TEPP-46 or control dimethyl sulfoxide (DMSO) ($n = 4$ biological replicates per group). **d**, Relative luminescence of HCT116 cells that were transfected with firefly luciferase HIF-1α reporter (p2.1) and Renilla luciferase constitutive reporter (pRL) and incubated for 24 h in the indicated conditions ($n = 6$ biological replicates per group for normoxia; $n = 3$ for hypoxia). **e**, ATP levels in HCT116 cells incubated for 24 h in the indicated conditions ($n = 3$ biological replicates per group). PKM2 activators DASA-58 and TEPP-46 were used at 50 μM in the culture medium. **f**, Relative duodenal villus length in mice of the indicated genotypes after four weeks of ad libitum $H_2O$ or HFCS. Mean villus length is reported relative to $H_2O$-treated controls for each genotype (mice per group: left to right: 5, 5, 5, 8, 6, 9). WT, wild type. **g**, Duodenal villi of wild-type mice that were treated for four weeks with the indicated diets. Scale bars, 200 μm. **h**, Change in serum triglyceride (TG) levels after an oral lipid bolus in mice treated through daily oral gavage for two weeks ($n = 8$ mice per group for $H_2O$ and HFCS; $n = 5$ for HFCS + TEPP-46). **i**, Representative intestines from $Apc^{Q1405X/+}$ mice treated with the indicated regimens and euthanized at 15 weeks old. Arrows indicate tumours. Scale bars, 2 mm. **j**, **k**, Total tumour area per histological section of large and small intestine (**j**) and red blood cell (RBC) count (**k**) in mice at 15 weeks (mice per group: left to right: 6, 5, 4, 6). **b**–**f**, **j**, **k**, Two-way ANOVA followed by Holm–Sidak post-hoc test for multiple comparisons; **h**, two-sided Student's *t*-test at the 4-h and 7-h time points. NS, not significant; $^*P < 0.05$, $^{**}P < 0.01$, $^{***}P < 0.001$, $^{****}P < 0.0001$. All data are mean ± s.e.m.

also protected from increased lipid uptake and fat accumulation after being fed with HFCS (Extended Data Fig. 9g–i).

Pharmacological activation of PKM2 also greatly modified the effects of fructose in the intestine. Even with doses far below those required to maintain effective serum levels of drug (2 mg per kg per day as opposed to 100 mg per kg per day)[7], mice that were treated with TEPP-46 had higher intestinal pyruvate kinase activity (Extended Data Fig. 9b) and were protected from the villus elongation induced by HFCS (Fig. 3g). We repeated this experiment using mice that were administered a once-daily oral gavage of HFCS to more closely approximate typical human consumption[15]. In this model, HFCS-fed mice developed villus elongation extending to the ileum by day 10 of treatment, and this could be prevented and reversed with concurrent administration of TEPP-46 (Extended Data Fig. 10a–c). As in the genetically altered mice, TEPP-46 protected against HFCS-induced increases in lipid absorption and fat accumulation (Fig. 3H, Extended Data Figs. 9h, 10d).

Given the effects of PK activation on normal epithelial tissue, we hypothesized that this approach might also inhibit the growth of intestinal tumours. Intestinal tumours originate from IECs both in the crypt and in the villus, so hypoxic stress may be a limiting factor in their development and progression[22]. Consistent with this theory, we observed high expression of PKM2 and other HIF-1α targets in primary human CRC tumours compared to normal adjacent epithelium (Extended Data Fig. 10e, f). In addition, the activity of pyruvate kinase in these tumours was inhibited relative to adjacent tissue (Extended Data Fig. 10g), potentially providing a survival advantage in hypoxia. In mouse intestinal tumours, we found regions of hypoxia in the core and along the periphery of the tumour, with many apoptotic cells, as well as upregulation of GLUT5 (Extended Data Fig. 10h–o). To test whether the activation of pyruvate kinase inhibits tumour growth, we fed HFCS with or without TEPP-46 to mice with a clinically relevant, tumour-predisposing mutation in one allele of the *Apc* gene ($Apc^{Q1405X/+}$)

(ref. [23]). In agreement with our previous findings[15], HFCS led to a more severe tumour burden and more profound anaemia—a complication that is associated with more severe disease and worse survival in this model and in humans. These changes were both prevented by treatment with a low dose of TEPP-46 (Fig. 3i–k, Extended Data Fig. 10p–r).

Together, these findings indicate that fructose promotes hypoxic cell survival in the intestine. This conclusion adds to a growing body of evidence indicating that fructose metabolism is an important component of oxygen sensing in diverse biological contexts[24,25]. For example, endogenously produced fructose is critical to the survival of the naked mole-rat in hypoxic burrows and critical in mouse cardiomyocytes after ischaemia, yet the mechanisms behind these interactions are poorly understood[26,27]. The finding that fructose-derived F1P inhibits PKM2, an important enzyme in hypoxia adaptation[5,6], offers additional insight into these observations. Given its relative scarcity in systemic circulation, endogenously produced fructose could serve as a highly specific signal for reprogramming cellular metabolism in response to hypoxia—a mechanism that we propose is leveraged (and targetable) when tissues such as intestinal villi and tumours are exposed to exogenous fructose. In addition, we find that the consequence of intestinal cell survival is an expansion of the intestinal surface area, which improves nutrient absorption. This finding may help to explain the growth-promoting effects of fructose in breast-fed infants, the increase in adiposity that occurs in fruit-foraging hibernating animals and the obesogenic properties of a Western-style diet[28,29].

## Online content

Any methods, additional references, Nature Research reporting summaries, source data, extended data, supplementary information, acknowledgements, peer review information; details of author contributions and competing interests; and statements of data and code availability are available at https://doi.org/10.1038/s41586-021-03827-2.


1. Bray, G. A., Nielsen, S. J. & Popkin, B. M. Consumption of high-fructose corn syrup in beverages may play a role in the epidemic of obesity. *Am. J. Clin. Nutr.* **79**, 537–543 (2004).
2. Joh, H.-K. et al. Simple sugar and sugar-sweetened beverage intake during adolescence and risk of colorectal cancer precursors. *Gastroenterology* **161**, 128–142 (2021).
3. Miller. M., Craig, J. W., Drucker, W. R. & Woodward, H. Jr. The metabolism of fructose in man. *Yale J. Biol. Med.* **29**, 335–360 (1956).
4. Jang, C. et al. The small intestine converts dietary fructose into glucose and organic acids. *Cell Metab.* **27**, 351–361 (2018).
5. Anastasiou, D. et al. Inhibition of pyruvate kinase M2 by reactive oxygen species contributes to cellular antioxidant responses. *Science* **334**, 1278–1283 (2011).
6. Nguyen, A. et al. PKLR promotes colorectal cancer liver colonization through induction of glutathione synthesis. *J. Clin. Invest.* **126**, 681–694 (2016).
7. Anastasiou, D. et al. Pyruvate kinase M2 activators promote tetramer formation and suppress tumorigenesis. *Nat. Chem. Biol.* **8**, 839–847 (2012).
8. Port, A. M., Ruth, M. R. & Istfan, N. W. Fructose consumption and cancer: is there a connection? *Curr. Opin. Endocrinol. Diabetes Obes.* **19**, 367–374 (2012).
9. Parikh, N. I. et al. Increasing trends in incidence of overweight and obesity over 5 decades. *Am. J. Med.* **120**, 242–250 (2007).
10. Liu, P. H. et al. Association of obesity with risk of early-onset colorectal cancer among women. *JAMA Oncol.* **5**, 37–44 (2019).
11. Siegel, R. L. et al. Colorectal cancer incidence patterns in the United States, 1974–2013. *J. Natl. Cancer Inst.* **109**, djw322 (2017).
12. Tasevska, N. et al. Sugars in diet and risk of cancer in the NIH-AARP Diet and Health Study. *Int. J. Cancer* **130**, 159–169 (2012).
13. Bostick, R. M. et al. Sugar, meat, and fat intake, and non-dietary risk factors for colon cancer incidence in Iowa women (United States). *Cancer Causes Control* **5**, 38–52 (1994).
14. Meyerhardt, J. A. et al. Dietary glycemic load and cancer recurrence and survival in patients with stage III colon cancer: findings from CALGB 89803. *J. Natl. Cancer Inst.* **104**, 1702–1711 (2012).
15. Goncalves, M. D. et al. High-fructose corn syrup enhances intestinal tumor growth in mice. *Science* **363**, 1345–1349 (2019).
16. Bu, P. et al. Aldolase B-mediated fructose metabolism drives metabolic reprogramming of colon cancer liver metastasis. *Cell Metab.* **27**, 1249–1262 (2018).
17. Hall, P. A., Coates, P. J., Ansari, B. & Hopwood, D. Regulation of cell number in the mammalian gastrointestinal tract: the importance of apoptosis. *J. Cell Sci.* **107**, 3569–3577 (1994).
18. Israelsen, W. J. & Vander Heiden, M. G. Pyruvate kinase: Function, regulation and role in cancer. *Semin. Cell Dev. Biol.* **43**, 43–51 (2015).
19. Yang, H., Wang, X., Xiong, X. & Yin, Y. Energy metabolism in intestinal epithelial cells during maturation along the crypt-villus axis. *Sci. Rep.* **6**, 31917 (2016).
20. Christofk, H. R., Vander Heiden, M. G., Wu, N., Asara, J. M. & Cantley, L. C. Pyruvate kinase M2 is a phosphotyrosine-binding protein. *Nature* **452**, 181–186 (2008).
21. Luo, W. et al. Pyruvate kinase M2 is a PHD3-stimulated coactivator for hypoxia-inducible factor 1. *Cell* **145**, 732–744 (2011).
22. Schwitalla, S. et al. Intestinal tumorigenesis initiated by dedifferentiation and acquisition of stem-cell-like properties. *Cell* **152**, 25–38 (2013).
23. Schatoff, E. M. et al. Distinct colorectal cancer–associated APC mutations dictate response to tankyrase inhibition. *Cancer Discov.* **9**, 1358–1371 (2019).
24. Kucharzewska, P., Christianson, H. C. & Belting, M. Global profiling of metabolic adaptation to hypoxic stress in human glioblastoma cells. *PLoS ONE* **10**, e0116740 (2015).
25. Armitage, E. G. et al. Metabolic profiling reveals potential metabolic markers associated with hypoxia inducible factor-mediated signalling in hypoxic cancer cells. *Sci. Rep.* **5**, 15649 (2015).
26. Mirtschink, P. et al. HIF-driven SF3B1 induces KHK-C to enforce fructolysis and heart disease. *Nature* **522**, 444–449 (2015).
27. Park, T. J. et al. Fructose-driven glycolysis supports anoxia resistance in the naked mole-rat. *Science* **356**, 307–311 (2017).
28. Goran, M. I., Martin, A. A., Alderete, T. L., Fujiwara, H. & Fields, D. A. Fructose in breast milk is positively associated with infant body composition at 6 months of age. *Nutrients* **9**, 146 (2017).
29. Denyes, A. & Carter, J. D. Utilization of acetate-1-C-14 by hepatic tissue from cold-exposed and hibernating hamsters. *Am. J. Physiol.* **200**, 1043–1046 (1961).



**Publisher's note** Springer Nature remains neutral with regard to jurisdictional claims in published maps and institutional affiliations.

© The Author(s), under exclusive licence to Springer Nature Limited 2021

# Methods

### Mice and diets

Six–eight-week-old male and female C57BL6/J, C57BL6/NJ, FVB and BALB/c mice were obtained from The Jackson Laboratory. Mixed-background male and female 'G5H' mice were provided by A. Dannenberg. *Vil1*$^{Cre/+}$;*Pkm*$^{tm1.1Mgvh/tm1.1Mgvh}$ (*Vil1*$^{Cre/+}$;*Pkm2*$^{f/f}$) mice were generated by crossing B6.Cg-Tg(*Vil1*$^{Cre/+}$)997Gum (stock number 004586) and B6;129S-*Pkm*$^{tm1.1Mgvh}$ (stock number 024048) mice purchased from The Jackson Laboratory. *Khk*$^{-/-}$ mice lacking both KHK-A and KHK-C on the C57BL/6J background were provided by D. Bonthron (University of Leeds) and M. Lanaspa and R. Johnson (University of Colorado)[30]. *Apc*$^{Q1405X/+}$ mice on the C57BL/6NJ background were provided by L. Dow (Weill Cornell Medical College)[23].

Unless otherwise indicated, all wild-type experiments used male C57BL/6J mice between the ages of 8 and 16 weeks. All genetically modified models (*Vil1*$^{Cre/+}$;*Pkm*$^{tm1.1Mgvh/tm1.1Mgvh}$, *Khk*$^{-/-}$, *Apc*$^{Q1405X/+}$) were equally weighted mixes of males and females between 10 and 20 weeks of age at the time of euthanasia.

Mice were maintained in temperature- and humidity-controlled specific-pathogen-free conditions on a 12-h light–dark cycle and received rodent chow (PicoLab Rodent 20 5053 LabDiet) and free access to drinking water. HFCS was prepared by combining D-(+)-glucose (Millipore Sigma, Cat. #G8270) and D-(−)-fructose (Millipore Sigma, F0127) in a 45:55 ratio using tap water. Match Purina 5053 fructose-free control (D17011901), high-fat (D19090601) and high-fat/high-sucrose (D19090602) diets were purchased from Research Diets. Age-matched cohorts were treated with HFCS either by ad libitum delivery in the drinking water (25% HFCS in tap water) or by once-daily oral gavage (45 mg glucose + 55 mg fructose, total 400 µl in tap water). Control mice were treated with tap water in the water bottle or 400 µl of tap water via daily oral gavage.

For drug trials, TEPP-46 (Millipore Sigma, 505487) dissolved in DMSO was added to the drinking water to a final concentration of 7.5 µg ml$^{-1}$ such that the total daily dose for a 30-g mouse consuming 8 ml of water daily was 2 mg kg$^{-1}$. Fluid consumption was monitored weekly to confirm that similar amounts of drug were consumed in each cage. Control mice received equal volumes of DMSO in the drinking water. For oral gavage, TEPP-46 was administered at 2 mg kg$^{-1}$ in HFCS or water. Control mice received an equal volume of DMSO dissolved in HFCS or water.

Male and female *Apc*$^{Q1405X/+}$ mice in a 1:1 ratio were initiated on their respective diets or treatments at 6 weeks and euthanized at 15 weeks of age. Other mice receiving treatment via the water bottle or diet were initiated on treatment at between 6 and 15 weeks of age and were euthanized after 4–6 weeks of intervention. Mice receiving oral gavage treatment were euthanized after 10–14 days of once-daily gavage. After euthanasia, tissues and intestines were collected, split into five sections (four of equal size for small intestine and one for the colon), Swiss-rolled and fixed in 4% paraformaldehyde (Santa Cruz Biotechnology, SC-281692) overnight at 4 °C. Tissues were then transferred to 70% ethanol and shipped to Histowiz for paraffin embedding, mounting, H&E staining and slide scanning at 40× magnification.

All animal studies were approved by the Institutional Animal Care and Use Committee (IACUC) of Weill Cornell Medical College and maintained as approved by the Institutional Animal Care and Use Committee (IACUC) at Weill Cornell Medicine under protocol number 2012-0074. Mice were regularly monitored for lethargy, gross weight loss, pallor and rectal prolapse. Mice that exhibited greater than 20% weight loss from peak weight, had red blood cell counts below $1 \times 10^9$ ml$^{-1}$ as determined from tail vein sampling or had rectal prolapse were euthanized. These limits were never reached in our experiments.

### Histological analysis

Scanned H&E images of small intestine from each trial were downloaded from Histowiz as ScanScope Virtual Slide (SVS) files and divided into separate files for duodenum, proximal jejunum, distal jejunum and ileum.

For manual villi analysis, each intestinal segment was further divided into 4 quadrants and 10 intact villi were measured from the distal edge of the crypt to the villi apex in each quadrant. A mean villus length was then calculated for the entire bowel segment.

For semi-automated analysis, SVS files were opened in ImageJ and the length of the intestinal section was measured using the freehand measurement tool (Extended Data Fig. 1a). Images were then stain-normalized to a standard H&E image using a custom MATLAB (release 2019b) script using a method described previously[31]. A random image from the set was then loaded into the MATLAB Colour Thresholder[32] and values were manually selected within the hue-saturation-value (HSV) colour space such that the intestinal villi, but not other tissues such as lymph nodes or pancreas, were selected (Extended Data Fig. 1b). These values were entered into a batch processing script that performed this villi segmentation on every image in the set. This resulted in binary images of pixels identified as villi and pixels identified as non-villi. The pixels occupied by villi were converted to area in µm$^2$ using the embedded scale from the original SVS file. The villi area was divided by the bowel segment length to yield the average thickness of the intestinal villi layer. This measurement correlated well with manual measurements of villi length and provided improved intra-operator or inter-operator variation (Extended Data Fig. 1c–g).

Polyp number and area were determined from SVS files analysed using ImageJ software in a blinded manner.

### Body composition and lipid tolerance

Body mass, fat mass and fat-free mass were measured and calculated using magnetic resonance spectroscopy using an EchoMRI Body Composition Analyzer as previously described[33]. Visceral fat and white adipose tissue were assessed by measuring the weight of the gonadal white adipose depot.

To assess lipid tolerance, mice were fasted for 8 h then administered 200 µl olive oil via oral gavage (Whole Foods, Extra Virgin – Cold Processed). Tail blood serum was collected over time and measured via enzymatic assay (see 'Biochemical analysis'). Mice resumed their diets after completion of the above testing and recovered for at least 48 h before euthanasia. To assess lipid absorption after blocking endogenous lipases, mice were treated with poloxamer 407 as previously described[34]. In brief, mice were fasted and then given an intraperitoneal injection of poloxamer 407. One hour later, triglyceride levels were measured from the serum and the mice were given a 200-µl oral olive oil bolus. Two hours later, serum triglyceride levels were measured again.

### Comprehensive metabolic monitoring

Metabolic monitoring was conducted using a Promethion Metabolic Screening System (Promethion High-Definition Multiplexed Respirometry System for Mice; Sable Systems International) as previously described[35]. In brief, rates of oxygen consumption ($VO_2$) and carbon dioxide production ($VCO_2$) were acquired by indirect calorimetry with a sampling frequency of 1 s. Respirometry values were determined every 5 min; the dwell time for each cage was 30 s, with baseline cage sampling frequency of 30 s occurring every four cages. Values of respiratory exchange ratio were calculated as ratios of $VCO_2$ to $VO_2$. Food intake and body mass were recorded continuously by gravimetric measurements within the cages. Physical activity was determined according to beam breaks within a grid of infrared sensors built into each cage. Energy expenditure was calculated using the Weir equation (energy expenditure = 3.941 kcal/l × $VO_2$ + 1.106 kcal/l × $VCO_2$)[36]. Energy expenditure is displayed as the total kcal per specified periods of time, with values adjusted by ANCOVA for body mass or corrected body mass using VassarStats.

### Faecal bomb calorimetry

Nutrient absorption was quantified as described previously[37]. Faecal pellets were collected from cage bottoms over 24 h, during which mice were single-caged and housed at 22 °C. Faecal pellets were dehydrated for 48 h and then subjected to bomb calorimetry using a Parr 6725 Semimicro Calorimeter.

### Immunohistochemistry and immunofluorescence

For BrdU tracing experiments, 100 µl of BrdU (100 mg $kg^{-1}$, Millipore Sigma, B5002) dissolved in sterile PBS (Corning, 21-040-CV) was injected intraperitoneally 72 h before mouse euthanasia as previously described[38]. For BrdU–EdU dual-labelling experiments, BrdU was injected 48 h before and EdU (10 mg $kg^{-1}$, Millpore Sigma, 900584) was injected 24 h before euthanasia. Pimonidazole, a 2-nitroimidazole that is reduced in hypoxic environments and then binds to thiol-containing proteins, was injected intraperitoneally 90 min before euthaniasia as per the manufacturer's instructions[39] (Hypoxyprobe, HP1-100Kit).

Immunohistochemistry was performed on formalin-fixed, paraffin-embedded tissues. Slides were deparaffinized with xylene and rehydrated in a graded ethanol series and water. Antigen retrieval was performed with 0.01 M citrate, pH 6.0 buffer by heating the samples in a pressure cooker for 10 min. Sections were blocked with avidin–biotin blocking for 30 min. Sections were incubated with primary antibody for 1 h at room temperature or overnight at 4 °C, followed by a 60-min incubation with biotinylated anti-rabbit IgG (goat, Vector Laboratories, PK6101, dilution 1:500) at room temperature for rabbit primaries. Mouse primaries on mouse tissues were assayed using a Mouse on Mouse Basic kit (Vector laboratories, BMK-2202) according to the manufacturer's instructions. Detection was performed with the DAB detection kit (Vector Laboratories, SK-4100) according to the manufacturer's instructions, followed by counterstaining with haematoxylin and cover slipping with Permount (Thermo Fisher Scientific, SP15-500).

Immunofluorescence was performed on formalin-fixed, paraffin-embedded tissues using the same method as above up to the application of the primary antibodies, which were incubated together. Slides were then washed in PBS and incubated with Alexa-Fluor-488- and Alexa-Fluor-568-conjugated secondary antibodies (Thermo Fisher Scientific, A21202 and A10042) as per the manufacturer's instructions. Slides were then washed and mounted with the TrueVIEW autofluorescence quenching kit with DAPI (Vector Laboratories, SP-8400-15) according to the manufacturer's instructions. Organoids were stained as described previously[40].

Antibodies used for immunohistochemistry and immunofluorescence included Ki-67 (rabbit, Abcam ab15580, dilution 1:500), CC3 (rabbit, Cell Signaling Technologies (CST) 9661, dilution 1:200), PKM1 (rabbit, CST 7067, dilution 1:600), PKM2 (rabbit, CST 4053, dilution 1:800), BrdU (mouse, Santa Cruz Biotechnology sc-32323, dilution 1:250), pimonidazole adducts (mouse, Hypoxyprobe Mouse-Mab, dilution 1:50), and SLC2A5 (GLUT5, mouse, Invitrogen MA1-036, 1:500). EdU was visualized using the ClickiT Plus EdU Alexa Fluor 647 Imaging Assay Kit (Thermo Fisher Scientific, C10340) according to the manufacturer's instructions.

For BrdU tracing analysis, the total villi length and the length from crypt to the BrdU-labelled cells furthest from the crypt were measured from 40–50 villi in the duodenums of each mouse using ImageScope software (Leica Biosystems). For BrdU–EdU dual-labelled tracing, the difference between the lengths of BrdU- and EdU-stained areas was divided by the time between these two injections.

TUNEL staining was performed on formalin-fixed, paraffin-embedded tissues by Histowiz.

### Imaging

Images of fluorescent-stained sections were acquired on a Zeiss LSM 880 laser scanning confocal microscope. Raw TIF files were processed using Fiji (Image J) and/or Photoshop CS (Adobe Systems) to create stacks, adjust levels and/or apply false colouring.

### Biochemical analysis

For measurement of hepatic triglyceride, frozen liver was weighed and digested in 6 volumes of alcoholic KOH (2:1 pure ethanol to 30% KOH) at 60 °C until the tissue was completely dissolved. Then 500 µl of digest was added to 540 µl of 1M $MgCl_2$ and mixed well. After a 10-min incubation on ice, samples were centrifuged for 30 min at maximum speed. The supernatant was aspirated into a new tube and glycerol content was measured using a calorimetric assay (Stanbio). This assay kit was also used to measure serum triglyceride.

Glucose and fructose concentration in cell culture media were measured with the EnzyChrom glucose assay kit (BioAssay Systems, EBGL-100) and EnzyChrom fructose assay kit (BioAssay Systems, EFRU-100). For lactate determination, a previously described spectrophotometric enzymatic assay was adapted for 96-well plates[41].

Pyruvate kinase activity was measured in recombinant protein and cell or tissue lysates in the presence of the indicated allosteric activators or small molecules by a previously described, lactate dehydrogenase (LDH)-coupled reaction in which PEP is converted by pyruvate kinase to pyruvate, which is then rapidly converted to lactate by LDH[42]. LDH consumes NADH and this rate of change was measured using a microplate spectrophotometer (BMG Labtech). Each allosteric regulator was tested in varying concentrations of PEP and the resulting graph of reaction rate versus PEP concentration was fitted to a substrate velocity curve to derive kinetic parameters under each condition. Substrate–velocity curves were plotted using Prism software (GraphPad Software). To calculate PK activity relative to maximum, activity was measured in tissue lysates before and after incubation for 1 h at 37 °C with 1 mM FBP, and the ratio of initial versus activated activity was calculated. Unless otherwise mentioned, the PEP concentration in the final reaction was 0.5 mM.

KHK activity was measured using a pyruvate kinase- and LDH-coupled reaction as previously described[43], with volumes adjusted for the 96-well plate format. Pyruvate and ADP were used as positive technical controls. The fructose concentration was 10 mM in each reaction.

### Cell lines, cell culture, virus preparations, transfections and culture additives

HCT116 and DLD1 cells were obtained from ATCC and cultured in DMEM (Corning, 10-013-CV) supplemented with 10% dialysed fetal bovine serum (dFBS) and 100 U $ml^{-1}$ penicillin and 100 µg $ml^{-1}$ streptomycin. All cells were cultured in a humidified incubator at 37 °C and 5% $CO_2$ unless otherwise stated. For assays not starting at confluence, the initial concentration of glucose was 25 mM. Cells were tested every two months for mycoplasma contamination. Hypoxia treatments were performed using a Forma Series 3 Water Jacketed $CO_2$ Incubator (Thermo Fisher Scientific). Oxygen was set to 2–4% depending on the meniscus height of the medium, using previously described calculations[44], to ensure consistent cellular oxygen deficit. Any manipulations to cells requiring more than a 5-min exposure to ambient oxygen were performed in a InvivO2 400 hypoxia workstation set to the appropriate oxygen level (The Baker Company).

For all hypoxia treatments the medium was supplemented to 10 mM with HEPES buffer (Corning, 25060CI). High cell density was defined as a seeding density of 1,000 cells per $mm^2$. Experiments were performed in 6-well, 12-well or 48-well plates using 3 ml, 2 ml, and 400 µl of medium, respectively; 96-well plates were avoided owing to large meniscus effects on the medium height in this small well format.

Glucose consumption rates in hypoxia for HCT116 and DLD1 cells were derived using medium samples from two different time points from confluent cells cultured in hypoxia. A known number of cells were plated the night before the experiment in 12-well plates, and confluence was confirmed the next morning. At the start of the experiment

the growth medium was aspirated, and the cells were gently washed with warm PBS. Then, fresh DMEM with or without 10 mM fructose was added to the culture dishes. Samples from the initial medium were then frozen at −20 °C. Forty-eight hours later, the medium was collected from each well and frozen at −20 °C. Medium samples were subsequently tested for sugar content by an enzymatic assay, and the difference in sugar concentration between the final and initial time points was calculated and divided by the time between time points to establish a rate of decrease. This was then divided by the number of cells plated to calculate the consumption per $10^6$ cells. Lactate production was calculated similarly using initial and final medium samples.

For experiments plated at confluence lasting longer than 24 h, cells were plated in 10 mM glucose and glucose was replenished at a rate of 15 µmol per day per $10^6$ initial cells unless otherwise noted. Cells used for metabolite labelling were plated at confluence in medium with 10 mM glucose ± 10 mM fructose. After 24 h, the cells were gently washed with warm PBS and given reduced-nutrient DMEM (Corning, 17-207-CV) supplemented with 5 mM glucose ± 5 mM fructose, 0.5 mM sodium pyruvate, 10 mM lactate, 1 mM glutamine and 10% dFBS to better simulate the tumour microenvironment during the final 8 h labelling period[45].

pLKO-shPKM2 was a gift from D. Anastasiou (Addgene, plasmid 42516) and scramble shRNA was a gift from D. Sabatini (Addgene, plasmid 1864). Lentiviruses were produced in 293T cells by co-transfection of plasmids expressing gag/pol, rev and vsvg with the respective pLKO. Selection was achieved with puromycin for at least 4 days. p2.1 and pRL-SV40 were procured from Addgene (Addgene, plasmids 27563 and 27163) and used as previously described[21]. Luciferase and Renilla activity were detected using the dual-luciferase reporter assay system (Promega, E1910) as per the manufacturer's instructions. TEPP-46 (Millipore Sigma, 505487) was used at 1 µM and 50 µM in recombinant and cell-culture experiments, respectively, unless otherwise stated. DASA-58 (MedChemExpress, HY-19330), was used at 50 µM. *N*-acetylcysteine (Millipore Sigma, A9165) was diluted in medium, pH-balanced to 7.4 and used at 2.5 mM.

### Cell confluence, viability assays, ThiolTracker and reactive oxygen species

Cell confluence, Annexin V Green (Essen BioScience, 4642), and Cytotox Red (Essen BioScience, 4632) measurements were conducted using an IncuCyte ZOOM Live Cell Analysis System (Essen BioScience) according to the manufacturer's instructions.

For Trypan Blue measurements, cells were trypsinized for 3 min at 37 °C and neutralized in complete medium. Resuspended cells were mixed 1:1 with Trypan Blue solution (Millipore Sigma, T8154) and analysed on a Cellometer Auto T4 bright field cell counter (Nexcelom Bioscience). For measurements of viability in adherent cells, the Cell Counting Kit-8 (Dojindo Molecular Technologies, CK04-05) was used according to the manufacturer's instructions.

For measurement of reduced thiols, confluent cell culture plates were incubated in hypoxia in reduced-nutrient DMEM (Corning, 17-207-CV) supplemented with 10% dFBS and 10 mM glucose or 5 mM glucose and 5 mM fructose. After 24 h, ThiolTracker Violet (Life Technologies, T10095) was used according to the manufacturer's instructions at 10 µM and plates were analysed on a Synergy Neo 2 plate reader (BioTek Instruments).

Total cell reactive oxygen species (ROS) measurements were performed using the ROS-Glo H2O2 assay (Promega, G8820) as per the manufacturer's instructions. Values from normoxic and hypoxic plates were compared after correcting for cell-independent changes in ROS-Glo measurements using wells containing only culture medium.

ATP measurements were acquired using the CellTiter-Glo Luminescent Cell Viability Assay (Promega, G7570) as per the manufacturer's instructions.

### Isolation and culture of intestinal organoids

Isolation, maintenance and staining of mouse intestinal organoids was performed as described previously[23]. For isolation, 15 cm of the proximal small intestine was removed and flushed with cold PBS. The intestine was then cut into 5-mm pieces, vigorously resuspended in 5 mmol $l^{-1}$ EDTA-PBS using a 10-ml pipette and placed at 4 °C on a benchtop roller for 10 min. This was then repeated for a second time for 30 min. After repeated mechanical disruption by pipette, released crypts were mixed with 10 ml DMEM basal medium (advanced DMEM/F12 containing penicillin–streptomycin, glutamine, 1 mmol $l^{-1}$ *N*-acetylcysteine containing 10 U $ml^{-1}$ DNase I (Roche, 04716728001), and filtered sequentially through 100-µm and 70-µm filters. FBS (1 ml; final 5%) was added to the filtrate and spun at 1,200 rpm for 4 min. The purified crypts were resuspended in basal medium and mixed 1:10 with growth-factor-reduced Matrigel (BD Biosciences, 354230). Forty microlitres of the resuspension was plated per well in a 48-well plate and placed in a 37 °C incubator to polymerize for 10 min. Small intestinal organoid growth medium (250 µl basal medium containing 50 ng $ml^{-1}$ EGF (Invitrogen, PMG8043), 50 nM LDN-193189 (Selleck Chemicals, S2618) and 500 ng $ml^{-1}$ R-spondin (R&D Systems, 3474-RS-050)) was then laid on top of the Matrigel. For subculture and maintenance, the medium was changed on organoids every two days and they were passaged 1:4 every 5 to 7 days. To passage, the growth medium was removed and the Matrigel was resuspended in cold PBS and transferred to a 15-ml Falcon tube. The organoids were mechanically disassociated using a P1000 or a P200 pipette and pipetting 50 to 100 times. Seven millilitres of cold PBS was added to the tube and pipetted 20 times to fully wash the cells. The cells were then centrifuged at 1,000 rpm for 5 min and the supernatant was aspirated. The cells were then resuspended in GFR Matrigel and replated as above. For freezing, after spinning the cells were resuspended in basal medium containing 10% FBS and 10% DMSO and stored in liquid nitrogen indefinitely.

For hypoxic organoid experiments, organoids from each independent line were dissociated and plated at a uniform density. After two days, the growth medium was changed to glucose-free basal medium supplemented with 10 mM glucose and 10 mM fructose, where indicated, and organoids were placed in normoxia, 4% $O_2$ or 1% $O_2$ conditions for 60 h at 37 °C. Every 24 h the concentration of glucose in the growth medium of each organoid well (3 ml total medium volume) was increased by 5 mM using sterile 1M glucose solution in a sealed hypoxia workstation. At the end of the hypoxic culture period, the medium was inoculated with EdU at 10 µM and organoids were returned to hypoxia to incubate for another 6 h. Then, medium samples were taken and frozen for later analysis of glucose and fructose depletion via enzymatic assay. Finally, the organoids were either dissociated and analysed via flow cytometry or fixed in-situ and analysed via confocal microscopy.

### Flow cytometry

Organoid EdU flow cytometry was performed using the ClickiT Plus EdU Alexa Fluor 647 Flow Cytometry Assay Kit (Thermo Fisher Scientific, C10634). Each well of a six-well plate was broken up by pipetting vigorously 50 times in 1 ml PBS, then diluted in 5 ml of PBS. Cells were pelleted at 1,100 rpm for 4 min at 4 °C, then resuspended in 50 µl TrypLE and incubated at 37 °C for 5 min. Five millilitres of PBS was then added to inactivate the TrypLE, and cells were pelleted. Cells were resuspended in 250 µl of 1% BSA in PBS, transferred to a 1.7-ml tube, and then pelleted at 3,000 rpm for 4 min. Cells were then stained with live/dead fixable green viability dye (Thermo Fisher Scientific, L34969) as per the manufacturer's instructions. Cells were then resuspended in 100 µl Click-iT fixative, and processed as instructed in the Click-iT Plus EdU protocol (starting with step 4.3). Wash and reaction volumes were 250 µl. After completion of staining, all cells from each well were resuspended in 250 µl 1% BSA in PBS and 200 µl of this suspension was analysed using an Attune NxT flow cytometer (Thermo Fisher Scientific). Viable and

proliferating cells were identified by the gating strategy depicted in Supplementary Fig. 4.

### Primary human tumour samples

Frozen primary human colon tumour and matched normal epithelium were obtained after informed consent from the WCMC Digestive Disease Registry, a protocol approved by the Weill Cornell Institutional Review Board. No protected health information was provided to the research team. After resection, tissue samples were immediately embedded in optimal cutting temperature compound and frozen in liquid nitrogen. Tumour areas were identified by a board-certified pathologist and six 2-mm cores were obtained from the frozen block. Cores were maintained at −80 °C prior to lysis and downstream analysis.

### Cell lysis and immunoblotting

Mouse tissues or pelleted cells were snap-frozen in a liquid nitrogen bath and stored at −80 °C until further processing. Lysis was performed in pyruvate kinase lysis buffer (50 mM Tris-HCl pH 7.5, 1 mM EDTA, 150 mM NaCl, 1% Igepal-630) supplemented freshly before usage with protease inhibitors (10 μg ml$^{-1}$ phenymethylsulfonyl fluoride, 4 μg ml$^{-1}$ aprotinin, 4 μg ml$^{-1}$ leupeptin and 4 μg ml$^{-1}$ pepstatin (pH 7.4)).

For immunoblotting, lysates were mixed with SDS–PAGE loading buffer (50 mM Tris-HCl pH 8.8, 1% w/v SDS, 2.5% glycerol, 0.001% w/v bromophenol blue and 143 mM β-mercaptoethanol) and heated to 70 °C for 10 min. Samples were separated by electrophoresis on 4–12% NuPAGE Bis-Tris gels (Invitrogen) and transferred to 0.45-μm PVDF membranes with wet transfer cells (Bio-Rad Laboratories). After 1 h of blocking with Tris-buffered saline with 0.1% (v/v) Tween 20 (TBST) containing 5% (w/v) BSA, membranes were incubated overnight at 4 °C with primary antibody in 5% BSA followed by a TBST wash and the appropriate secondary antibody (1:6,000) for 1h at room temperature. Signal was detected using an Odyssey CLx imaging system (LI-COR).

### Antibodies

In alphabetical order [target (species (Rb; rabbit; Ms, mouse), manufacturer, catalogue number, western blot dilution, IHC dilution (if applicable))]: ACC (Rb, CST, 3676, 1:1,000), pACC(s79) (Rb, CST, 3661, 1:1,000), aldolase A (Rb, CST, 8060, 1:1,000), aldolase B (Rb, Abcam, 153828, 1:1,000, 1:1,000), AMPKa (Rb, CST, 2532, 1:1,000), pAMPK (t172) (Rb, CST, 2535, 1:1,000), α-tubulin (Ms, CST, 3873, 1:1,000), β-actin (Ms, Abcam, 6276, 1:1,000), BCL-2 (Rb, CST, 2876, 1:1,000), BCL-XL (Rb, CST, 2764, 1:1,000), BrdU (IIB5) (Ms, SC, sc-32323, 1:1,000, 1:250), CC3 (Rb, CST, 9661, 1:1,000, 1:200), enolase 1 (Rb, CST, 3810, 1:1,000), GLUT5 (Ms, Invitrogen, MA1-036, 1:1,000), GLUT5 (Ms, SC, 271055, 1:1,000), HIF-1α (Rb, CST, 36169, 1:1,000), HK1 (Rb, CST, 2024, 1:1,000), HK2 (Rb, CST, 2867, 1:1,000), Hypoxyprobe (Ms, HP, Mouse-Mab, 1:1,000, 1:50), KHK (Rb, Abcam, 154405, 1:1,000, 1:500), KHK-A (Rb, SAB, 21708, 1:1,000, 1:500), KHK-C (Rb, SAB, 21709, 1:1,000, 1:500), LDHA (Rb, CST, 2012, 1:1,000), MCL-1 (Rb, CST, 5453, 1:1,000), pBAD (S136) (Rb, CST, 4366, 1:1,000), PDH (Rb, CST, 3205, 1:1,000), pPDH (s293) (Rb, CST, 31866, 1:1,000), PKLR (Rb, Abcam, 171744, 1:1,000), PKM1 (Rb, CST, 7067, 1:1,000, 1:600), PKM2 (Rb, CST, 4053, 1:1,000, 1:800). CST, Cell Signaling Technologies; SC, Santa Cruz Biotechnology; HP, Hypoxyprobe; SAB, Signallway Antibody.

### Metabolomics analysis

Polar metabolites were extracted from cell pellets using a 40:40:20 mixture of ice-cold acetonitrile:methanol:water with 0.1M formic acid. Samples were then centrifuged at 4 °C for 15 min at 14,000 rpm. Supernatants were then evaporated and resuspended in deionized water for LC–MS analysis.

Quantitative metabolome analysis was performed as described previously[15]. In brief, aqueous tissue extracts were separated by liquid chromatography on an Agilent 1290 Infinity LC system by injection of 10 μl of filtered extract through an Agilent ZORBAX Extend C18, 2.1 × 150 mm, 1.8 μm (Agilent Technologies) downstream of an Agilent ZORBAX SB-C8, 2.1 mm × 30 mm, 3.5 μm (Agilent Technologies) guard column heated to 40 °C. Solvent A (97% water/3% methanol containing 5 mM tetrabutylammonium hydroxide (TBA) and 5.5 mM acetic acid) and Solvent B (methanol containing 5 mM TBA and 5.5 mM acetic acid) were infused at a flow rate of 0.250 ml min$^{-1}$. The 24-min reverse phase gradient was as follows: 0–3.5 min, 0% B; 4–7.5 min, 30% B; 8–15 min, 35% B; 20–24 min, 99% B; followed by a 7-min post-run at 0% B. Acquisition was performed on an Agilent 6230 TOF mass spectrometer (Agilent Technologies) using an Agilent Jet Stream electrospray ionization source (Agilent Technologies) operated at 4,000 V Cap and 2,000 V nozzle voltage in high-resolution, negative mode. The following settings were used for acquisition: The sample nebulizer set to 45 psig with sheath gas flow of 12 l min$^{-1}$ at 400 °C. Drying gas was kept at 325 °C at 8 l min$^{-1}$. Fragmentor was set to 125 V, with the skimmer set to 50 V and Octopole Vpp at 400 V. Samples were acquired in centroid mode for 1.5 spectra/s for $m/z$ values from 50 to 1,500.

Collected data from the above methods was analysed by XCMS and X13CMS[46,47]. Metabolites were identified from ($m/z$, rt) pairs by both retention time comparison with authentic standards and expected isotopomer distributions. When indicated, cells were treated with D-[U-13C6]-glucose, D-[U-13C6]-fructose, L-[U-13C5]-glutamine, or L-[U-13C3]-lactate in place of the unlabelled nutrient (Cambridge Isotope Laboratories). Labelling proceeded for 8 h.

The various fatty acids are represented by "Cx:y", where x denotes the number of carbons and y the number of double bonds. For example, the symbol for palmitic acid is C16:0 and palmitoleic acid is C16:1.

### RNA extraction

Total RNA was extracted from frozen cell pellets using the RNeasy Mini Kit (Qiagen) and following the manufacturer's instructions. In brief, cells were lysed using Buffer RLT supplemented with 1% (v/v) β-mercaptoethanol and QIAshredder columns (Qiagen) were subsequently used to homogenize the cell lysates. To remove contaminating genomic DNA, on-column digestion with DNase I was performed using the RNase-free DNase Set (Qiagen) as per the manufacturer's instructions.

### KHK amplicon generation

Targeted isoform sequencing is a highly specific, amplification-based method used to characterize the diversity of expressed isoforms at a particular gene locus. In brief, 100 ng of high-quality, DNase-treated total RNA was primed with an oligodT primer and reverse-transcribed into single-stranded cDNA using the SuperScript IV First-Strand Synthesis System (Thermo Fisher Scientific). The reverse transcription (RT) reaction was treated with ribonuclease H (RNaseH) to remove any remaining RNA templates. The single-stranded cDNA was then supplied at 5% of the total PCR reaction volume of targeted amplification using KHK-specific primers and TaKaRa LA Taq Polymerase with GC Buffer I (Clontech). Three separate PCR reactions were performed per sample using three unique reverse primers designed at alternate 3′ exons based on NCBI reference annotations of KHK. The resulting full-length cDNA amplicons were then purified of excess nucleotides, adaptor dimers and buffers using 1× AMPure PB beads (Pacific Biosciences).

KHK primer sequences [primer name (primer sequence 5′ → 3′)]: human KHK_F_cds (ATGGAAGAGAAGCAGATCCTGTG), human KHK_R_cds (TCACACGATGCCATCAAAG), human KHK_R_altCDS (TCACCCTAGCAGCCCCC), human KHK_R_altCDS_ex5 (CCTCATTCTGCAGAGGAAAA).

### PacBio library preparation and sequencing

The purified, full-length cDNA amplicons were then prepped for PacBio single-molecule real-time (SMRT) sequencing using the Express Template Preparation Kit 2.0 (Pacific Biosciences) and following the manufacturer's instructions. In brif, 100 ng of cDNA from each sample was

treated with a DNA damage repair enzyme mix to repair nicked DNA, followed by an end repair and A-tailing reaction to repair blunt ends and polyadenylate each template. Next, barcoded overhang SMRTbell adapters were ligated onto each template and purified using 1× AMPure PB beads to remove small fragments and excess reagents (Pacific Biosciences). The completed SMRTbell libraries were further treated with the SMRTbell Enzyme Clean Up Kit to remove unligated templates and then were equimolar pooled. The final pooled library was then annealed to sequencing primer v4 and bound to sequencing polymerase 3.0 before being sequenced on one SMRTcell 1M on the Sequel I system with a 20-h movie.

### Targeted IsoSeq analysis

After data collection, the raw sequencing subreads were imported into the SMRTLink 9.0 bioinformatics tool suite (Pacific Biosciences) for processing. Intramolecular error correcting was performed using the circular consensus sequencing (CCS) algorithm to produce highly accurate (above Q20) CCS reads, each requiring a minimum of three polymerase passes. The CCS reads were then passed to the lima tool to remove barcode sequences and orient the isoforms into the correct sense or antisense direction. The refine tool was then used to remove concatemers from the full-length reads, resulting in final consensus isoforms ready for downstream analysis. The full-length, non-chimaeric (FLNC) reads were subsequently aligned to the GRCh38 reference genome using GMAP (v.2020-09-12), a splice-aware aligner specifically designed to handle long-read cDNA sequences. Redundant transcripts were then collapsed down to representative isoforms by passing the uniquely mapped isoforms through the TAMA Collapse algorithm with default parameters. The representative isoforms were further processed using the SQANTI3 (v.1.6) tool suite, which identifies and removes RT-switching and intra-priming artefacts. The filtered isoforms were then annotated using SQANTI3 by comparing each isoform to the NCBI RefSeq gene annotation database and categorized as either a known or novel transcript of KHK. Novel isoforms were defined as having at least one novel splice junction not previously annotated by NCBI. Isoforms with more than one FLNC supporting read from each sample were then merged together using the TAMA Merge algorithm to form one final isoform set representing all isoforms expressed across all samples.

### Production of recombinant pyruvate kinase

Human PKM1, PKM2 and its mutants were cloned into a pET28a vector (Novagen) at NdeI and BamHI sites and expressed as an N-terminal His6 tag fusion protein. The protein was expressed and purified by standard protocol. In brief, pET28a-PKM2 was transformed into BL21(DE3)pLysS cells and grown to an absorbance of 0.8 at 600 nm, then induced with 0.5 mM IPTG for 7 h at room temperature. Cells were lysed by lysozyme in lysis buffer (50 mM Tris pH 8.0, 10 mM MgCl2, 200 mM NaCl, 100 mM KCl, 20% glycerol, 10 mM imidazole, 1 mM PMSF) and cell lysate was cleared by centrifugation. Enzyme was purified by batch binding to Ni-NTA resin (Qiagen). The resin was then washed with lysis buffer containing 30 mM imidazole for 200 column volumes, and His6-tagged PKM2 was eluted with 250 mM imidazole. The protein was dialysed overnight at 4 °C to remove the imidazole. Human PKL was purchased from R&D Systems (8569-PK).

### Density gradient ultracentrifugation, cross-linking and size-exclusion chromatography

Sucrose gradients were formed and analysed as described in detail elsewhere[48]. In brief, 10 ml 10–40% sucrose gradients were created using a Gradient Master (BioComp Instruments) with the indicated metabolites evenly distributed throughout the gradient at a concentration of 1 mM. Subsequently, 400 µg of recombinant protein was incubated with the indicated metabolites at 1mM for 30 min at 25 °C, then gently layered atop the gradients. The gradients were then centrifuged for 16 h at 4 °C and 237,000*g* in an SW 55 Ti rotor and Beckman L-80 ultracentrifuge. A piston gradient fractionator (BioComp instruments) was then used to fractionate the separated protein complexes which were then analysed by western blot.

For cross-linking, purified recombinant enzyme at a concentration of 10 µg ml$^{-1}$ in 1× pyruvate kinase dilution buffer (50 mM Tris-HCl pH 7.5, 100 mM KCl and 5 mM $MgCl_2$) was incubated with the indicated metabolites for 30 min at 37 °C. Then, di(*N*-succinimidyl) glutarate (Millipore Sigma) was added to a final concentration of 1mM and incubated for 10 min at 25 °C. The reaction was quenched with 1M Tris-HCl to a final concentration of 50 mM and samples were analysed by SDS–PAGE and immunoblotting as previously described.

For size-exclusion chromatography, recombinant PKM2 was incubated alone or with FBP (100 µM) or F1P (500 µM) for one hour in PK dilution buffer (50 mM Tris-HCl pH 7.5, 100 mM KCl and 5 mM $MgCl_2$) on ice. Protein was then run on a Superdex 200 Increase 10/300 column (GE Life Sciences) equilibrated with the same buffer and metabolite, and 0.5-ml fractions were collected and subjected to SDS–PAGE and Coomassie blue staining.

### Pyruvate kinase docking simulations

The crystal structure of PKM2[20] was used to perform docking simulations for F1P using the Maestro software package (release 2019-2, Schrödinger).

### Statistics and reproducibility

Statistical analyses were conducted using GraphPad Prism (v.9.1). Data are mean ± s.e.m. unless stated otherwise. Exact *P* values are provided with the Source Data. Experiments were repeated independently, with similar results obtained. Mouse cohort sizes were informed by a priori power calculations using the variation from initial villus investigations with the aid of G*Power software (G*Power, v.3.1). Mice were randomly assigned to treatment groups. Investigators were blinded during image analysis of villus length and tumour burden. Investigators were not blinded to allocation during experiments.

### Reporting summary

Further information on research design is available in the Nature Research Reporting Summary linked to this paper.

## Data availability

Additional data that support the findings of this study are available from the corresponding author upon reasonable request. Source data are provided with this paper.

## Code availability

Villi analysis code, licensing information, and instructions for use are available at https://github.com/sam-taylor/VilliQuant.


30. Diggle, C. P. et al. Ketohexokinase: expression and localization of the principal fructose-metabolizing enzyme. *J. Histochem. Cytochem.* **57**, 763–774 (2009).
31. Macenko, M. et al. A method for normalizing histology slides for quantitative analysis. In *2009 IEEE International Symposium on Biomedical Imaging: From Nano to Macro* 1107–1110 (IEEE, 2009).
32. MATLAB v.9.7.0.1190202 (R2019b) (The MathWorks Inc., 2018).
33. Mystkowski, P. et al. Validation of whole-body magnetic resonance spectroscopy as a tool to assess murine body composition. *Int. J. Obes.* **24**, 719–724 (2000).
34. Millar, J. S., Cromley, D. A., McCoy, M. G., Rader, D. J. & Billheimer, J. T. Determining hepatic triglyceride production in mice: comparison of poloxamer 407 with Triton WR-1339. *J. Lipid Res.* **46**, 2023–2028 (2005).
35. Krisko, T. I. et al. Dissociation of adaptive thermogenesis from glucose homeostasis in microbiome-deficient mice. *Cell Metab.* **31**, 592–604 (2020).
36. Weir, J. B. New methods for calculating metabolic rate with special reference to protein metabolism. *J. Physiol.* **109**, 1–9 (1949).
37. Staffas, A. et al. Nutritional support from the intestinal microbiota improves hematopoietic reconstitution after bone marrow transplantation in mice. *Cell Host Microbe* **23**, 447–457 (2018).

38. Nalapareddy, K. et al. Canonical Wnt signaling ameliorates aging of intestinal stem cells. *Cell Rep*. **18**, 2608–2621 (2017).
39. Raleigh, J. A. & Koch, C. J. Importance of thiols in the reductive binding of 2-nitroimidazoles to macromolecules. *Biochem. Pharmacol*. **40**, 2457–2464 (1990).
40. O'Rourke, K. P., Dow, L. E. & Lowe, S. W. Immunofluorescent staining of mouse intestinal stem cells. *Bio Protoc*. **6**, e1732 (2016).
41. White, R., Yaeger, D. & Stavrianeas, S. Determination of blood lactate concentration: reliability and validity of a lactate oxidase-based method. *Int. J. Exerc. Sci*. **2**, 2 (2009).
42. Ashizawa, K., McPhie, P., Lin, K.-H. & Cheng, S.-Y. An in vitro novel mechanism of regulating the activity of pyruvate kinase M2 by thyroid hormone and fructose 1, 6-bisphosphate. *Biochemistry* **30**, 7105–7111 (1991).
43. Adelman, R. C., Ballard, F. J. & Weinhouse, S. Purification and properties of rat liver fructokinase. *J. Biol. Chem*. **242**, 3360–3365 (1967).
44. Al-Ani, A. et al. Oxygenation in cell culture: Critical parameters for reproducibility are routinely not reported. *PLoS ONE* **13**, e0204269 (2018).
45. Sullivan, M. R. et al. Quantification of microenvironmental metabolites in murine cancers reveals determinants of tumor nutrient availability. *eLife* **8**, e44235 (2019).
46. Smith, C. A., Want, E. J., O'Maille, G., Abagyan, R. & Siuzdak, G. XCMS: processing mass spectrometry data for metabolite profiling using nonlinear peak alignment, matching, and identification. *Anal. Chem*. **78**, 779–787 (2006).
47. Huang, X. et al. X13CMS: global tracking of isotopic labels in untargeted metabolomics. *Anal. Chem*. **86**, 1632–1639 (2014).
48. Fernandez-Martinez, J., Lacava, J. & Rout, M. P. Density gradient ultracentrifugation to isolate endogenous protein complexes after affinity capture. *Cold Spring Harb. Protoc*. https://doi.org/10.1101/pdb.prot087957 (2016).

**Acknowledgements** We acknowledge C. Gurbatri for her assistance in figure preparation, M. Lyashenko for his technical assistance with experiment replication and Y.-T. Chen for his pathological review of the primary human CRC tissue. We thank J. Yun for her discussions, which informed the early development of this work. *Khk*$^{-/-}$ mice were provided by D. T. Bonthron and R. J. Johnson. *Glut5*$^{-/-}$ mice were provided by R.P. Ferraris and St. Jude's Children's Research Hospital. S.R.T. and E.M.S. were supported by a Medical Scientist Training Program grant from the National Institute of General Medical Sciences of the National Institutes of Health under award number T32GM007739 to the Weill Cornell–Rockefeller–Sloan Kettering Tri-Institutional MD–PhD Program. This work was supported by NIH R35 CA197588 (L.C.C.), SU2C-AACR-DT22-17 (L.C.C.), NIH K08 CA230318 (M.D.G.), R25 AI140472 (K.Y.R.), a grant from the Lung Cancer Research Foundation and institutional funds from Weill Cornell Medicine.

**Author contributions** S.R.T. and M.D.G. contributed to the conception and design of the study. S.R.T., A.J.D., L.E.D., K.Y.R., L.C.C. and M.D.G. contributed ideas that formulated the overarching research goals and aims. E.M.S. and L.E.D. generated and provided the *Apc*$^{Q1405X/+}$ mouse model and guided its experimental use. S.R.T., N.V. and J.L.J. contributed to the structural and biochemical assays of pyruvate kinase. M.A.S. collected and provided the primary human tumour samples. A.J.D. provided the *Glut5*$^{-/-}$ mouse model and ideas that guided the initial phenotyping of the wild-type mice that were fed fructose. S.R.T., S.R. and N.J.F. performed programming, software development and implementation of the computer code and supporting algorithms. S.R.T., S.R. and S.-K.H. conducted mouse physiology studies and performed necropsy and tissue analysis. S.R.T. and A.K. performed the mouse intestinal organoid experiments under the guidance of L.E.D. S.R.T. and N.N. performed and analysed the LC–MS metabolomics experiments under the guidance of K.Y.R. and M.D.G. R.J.L. performed mutagenesis and generated recombinant pyruvate kinase. R.P. performed KHK activity assays. R.P.S. assisted with targeted isoform sequencing. S.R.T. performed all other experiments. S.R.T. and M.D.G. wrote the manuscript and verified the overall replication and reproducibility of results, experiments and other research outputs.

**Competing interests** L.C.C. is a founder, shareholder and member of the scientific advisory board of Agios Pharmaceuticals and a founder and former member of the scientific advisory board of Ravenna Pharmaceuticals (previously Petra Pharmaceuticals). These companies are developing therapies for cancer. L.C.C. has received research funding from Ravenna Pharmaceuticals. L.C.C. and M.D.G. are co-founders and shareholders of Faeth Therapeutics, which is developing therapies for cancer. M.D.G. has received speaking and/or consulting fees from Pfizer, Novartis, Petra Pharmaceuticals, Faeth Therapeutics and TruMacro Nutrition. The laboratory of M.D.G. has received financial support from Pfizer. All other authors report no competing interests.

**Additional information**

**Supplementary information** The online version contains supplementary material available at https://doi.org/10.1038/s41586-021-03827-2.

**Correspondence and requests for materials** should be addressed to M.D.G.

**Peer review information** *Nature* thanks Dimitrios Anastasiou, M. Mahmood Hussain and the other, anonymous, reviewer(s) for their contribution to the peer review of this work.

**Reprints and permissions information** is available at http://www.nature.com/reprints.

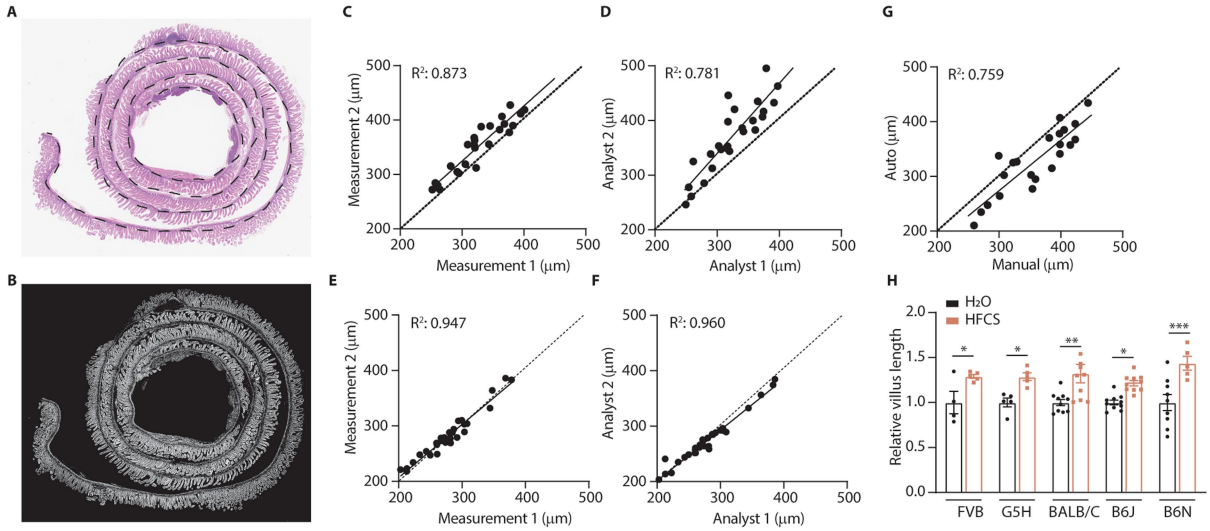


**Extended Data Fig. 1 | Image segmentation avoids the pitfalls of manual villi measurement. a**, Stain-normalized H&E images of Swiss-rolled intestines were loaded into image-analysis software, which was used to manually measure the length of the gut section (dotted black line). **b**, Image segmentation isolates villi (white) while excluding other tissues such as lymph nodes, pancreas and intestinal crypts. **c**, Intra-operator variation is a source of measurement error in manual villi measurements. The *x* and *y* axes represent measurements taken by the same analyst at different times. **d**, Inter-operator variation is another source of measurement error in manual villi measurements. The *x* and *y* axes represent measurements taken by different analysts. **e**, **f**, Intra- and inter-operator variation are minimized when using the semi-automated protocol. The comparisons in **e**, **f** are the same as in **c**, **d**; however, the only manual measurement in the semi-automated method is the measurement of the whole gut section length. **g**, Automated and manual measurements correlate. The *x* and *y* axes represent measurements obtained from the manual and semi-automated protocols, respectively. **h**, Mice from various genetic backgrounds were fed HFCS and the mean villus length in the duodenal intestinal epithelium was measured using a custom analysis algorithm (mice per group: left to right ($H_2O$|HFCS): 4|5, 5|5, 10|10, 10|10, 9|5). **c**–**g**, Each point represents a distinct image; dotted line: unity; $R_2$ is displayed for the linear regression fit of the data. **h**, Two-way ANOVA followed by Holm–Sidak post-hoc test for multiple comparisons. $^*P < 0.05$, $^{**}P < 0.01$, $^{***}P < 0.001$. Error bars represent ± s.e.m. See Source Data for exact *P* values for all figures.

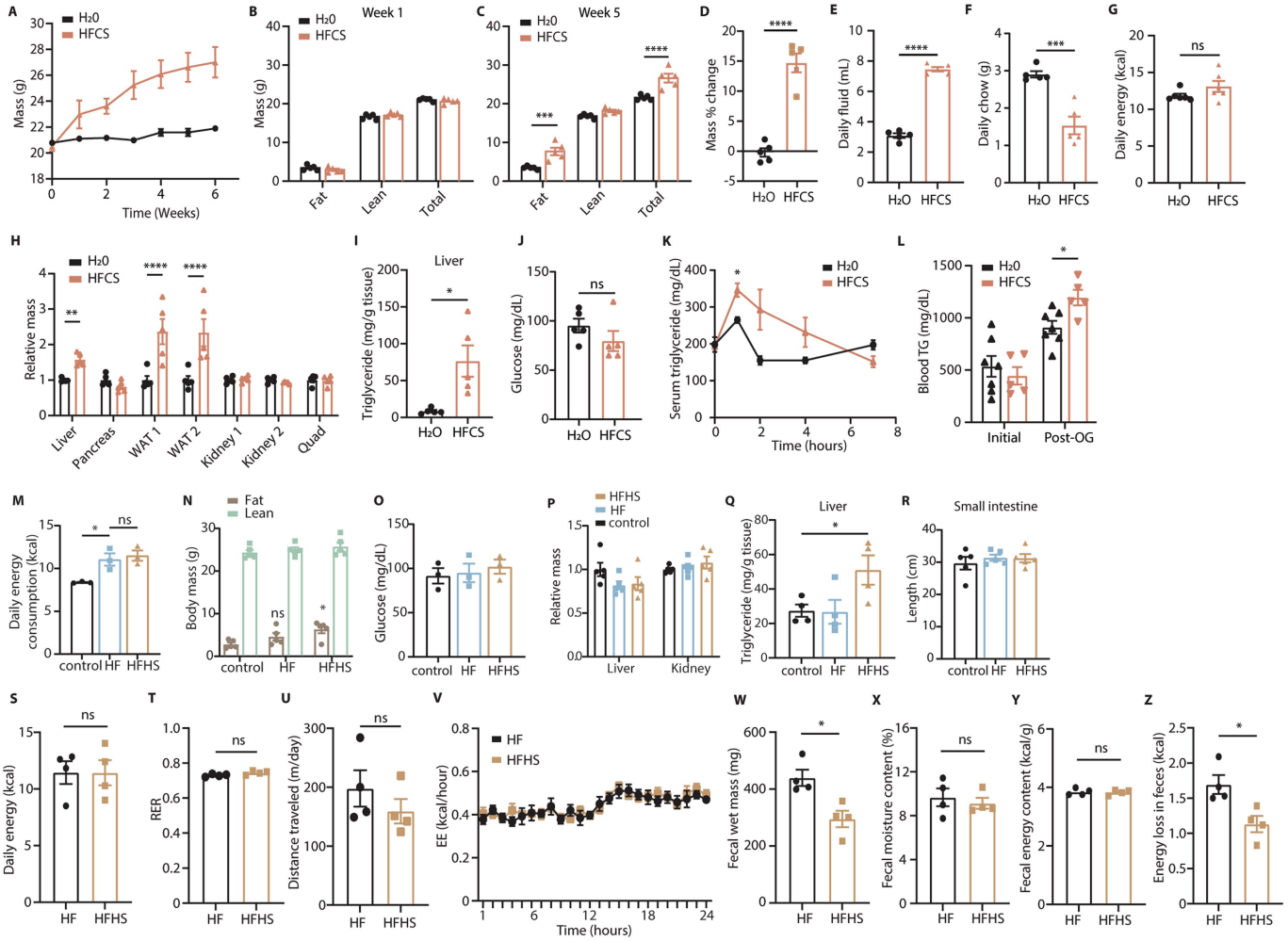


**Extended Data Fig. 2 | Dietary fructose promotes weight gain and adiposity independent of caloric intake. a**, Mice fed normal chow with or without 25% HFCS ad libitum were weighed weekly for six weeks. **b**–**d**, Total, lean and fat body mass were measured before and five weeks after mice were placed on diets. **e**–**g**, Total consumption of chow and fluid was measured weekly to calculate caloric consumption ($n = 5$ serial measurements per group). **h**, **i**, Tissues from mice on the indicated diets were collected and weighed and the liver was assayed for triglyceride content. WAT, white adipose tissue from the left or right gonadal fat depot. **j**, After five weeks, mice were fasted and blood glucose was measured by glucometer (**a**–**j**, 5 mice per group). **k**, A lipid tolerance test was performed on wild-type female mice fed HFCS ($n = 3$ mice per group). **l**, Mice treated with water or HFCS were fasted and then given an intraperitoneal injection of poloxamer 407. One hour later, triglyceride levels were measured from the serum and the mice were given an oral olive oil bolus. Two hours later, serum triglyceride levels were measured again ($n = 7$ ($H_2O$) and $n = 5$ (HFCS) mice per group). **m**, Mice fed fructose-free control diets (control), high-fat diets consisting of 45% kcal from fat (HF), and high-fat diets with sucrose in place of glucose as the main sugar (HFHS) were monitored weekly for chow consumption by cage ($n = 3$ repeated measurements per group). **n**, Total, lean and fat body mass were measured after five weeks on the diet. Statistical comparisons are made against control fat mass ($n = 5$ mice per group). **o**, After four weeks on the diet, mice were fasted and blood glucose was measured with a glucometer ($n = 3$ mice per group). **p**–**r**, After euthanasia, tissues were collected and weighed, liver tissue was homogenized and assayed for triglyceride content, mouse intestines were excised en bloc and the intestinal length was measured using ImageJ software ($n = 5$ (**p**, **r**) and $n = 4$ (**q**) mice per group). **s**, Mice treated with high-fat or high-fat high-sucrose diets for two weeks were housed in metabolic cages and food intake over 24 h was measured. **t**, $O_2$ consumption and $CO_2$ production were measured to calculate the respiratory exchange ratio. **u**, **v**, Total distance travelled was also measured (**u**), as was hourly energy expenditure (**v**), which was calculated using the Weir equation[8]. **w**–**z**, Mice were individually housed and faecal matter was collected over a 24-h period (**w**), dried (**x**) and then analysed by bomb calorimetry to measure energy content and energy loss over the collection period (**y**, **z**) (**s**–**z**, 4 mice per group). **b**, **c**, **h**, **n**, Two-way ANOVA followed by Holm–Sidak post-hoc test for multiple comparisons; **d**–**g**, **i**, **j**, **l**, **s**–**u**, **w**–**z**, Student's two-sided *t*-test; **k**, **m**, **o**, **q**, one-way ANOVA followed by Holm–Sidak post-hoc test for multiple comparisons. NS, not significant; $^*P < 0.05$, $^{**}P < 0.01$, $^{***}P < 0.001$, $^{****}P < 0.0001$. All data are mean ± s.e.m.

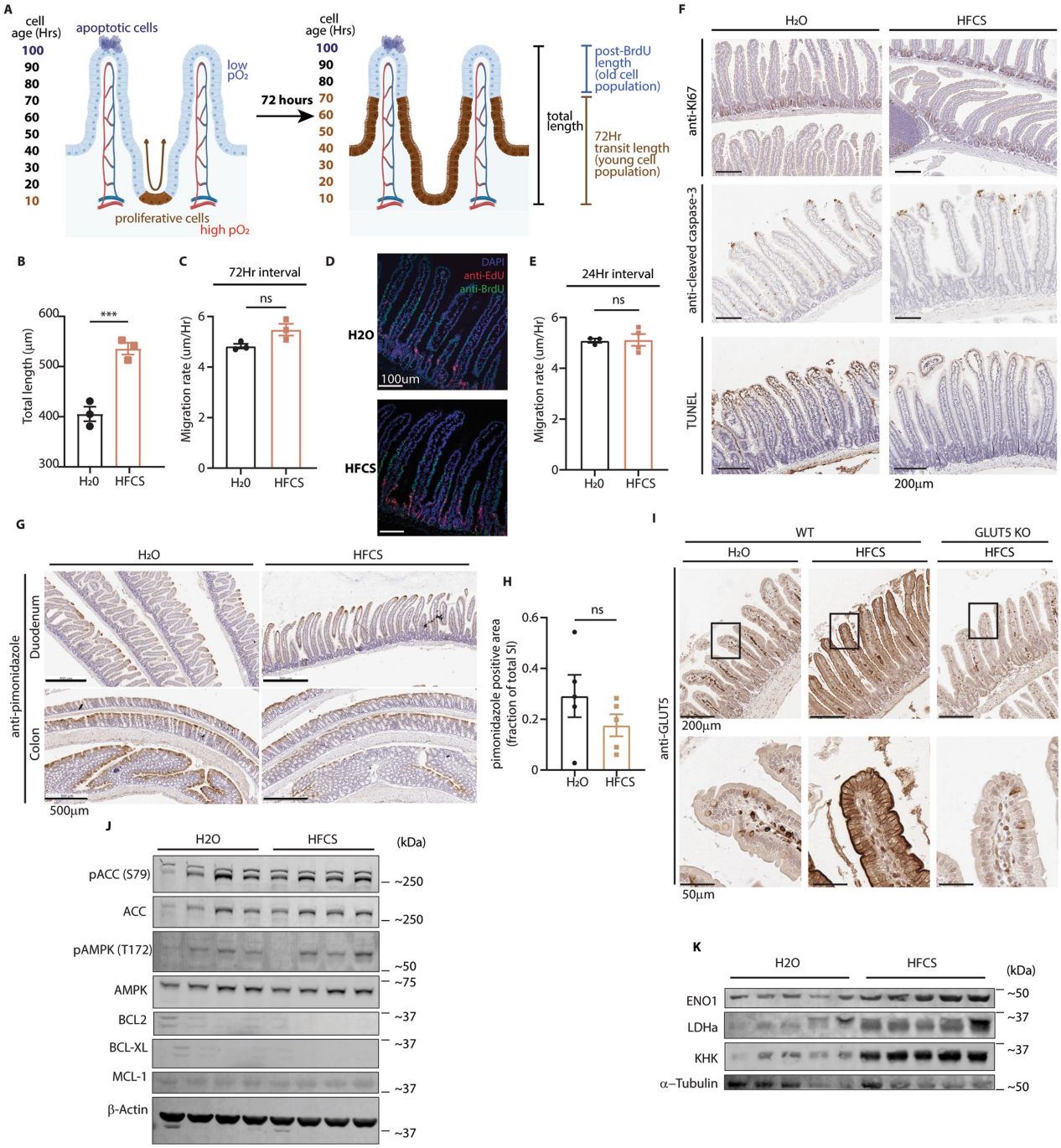


**Extended Data Fig. 3** | See next page for caption.

**Extended Data Fig. 3 | HFCS increases villus survival and expression of GLUT5 and HIF target proteins. a**, Model depicting the strategy of the BrdU tracing experiment. BrdU labels cells synthesizing DNA (brown). These cells transit up the length of the villus and away from richly oxygenated blood in 3–4 days. Unlabelled cells beyond the BrdU front at the time that mice were euthanized were thus generated before BrdU injection. **b**, Duodenal villus length was measured from H&E images from $H_2O$- and HFCS-treated mouse intestine ($n = 3$ mice per group, 40 villi per mouse). **c**, Mice were administered BrdU 72 h before euthanasia, and intestines were then examined by IHC. The length of BrdU-labelled regions of the villus was measured in both treatment groups and this length was divided by the interval between injection and euthanasia to yield migration rate ($n = 3$ mice per group, 15–20 duodenal villi per mouse). **d**, **e**, In a separate experiment, mice were treated with $H_2O$ or HFCS and given BrdU (green) 48 h before and EdU (red) 24 h before euthanasia. Duodenal villi were then stained and imaged by immunofluorescence and analysed as in **c**. The difference between the BrdU and EdU lengths was divided by the interval between injections to yield the migration rate ($n = 3$ ($H_2O$) and $n = 4$ (HFCS) mice per group, 15–20 duodenal villi per mouse). Scale bars, 100 μm. **f**, Mice treated with $H_2O$ or 25% HFCS were euthanized and the intestines were examined by IHC against Ki-67, CC3 and TUNEL. Scale bars, 200 μm. **g**, Before euthanasia, mice treated as in **f** were injected with pimonidazole to label tissue hypoxia. Intestines were then fixed and examined for pimonidazole intensity by IHC. Representative images are shown. Scale bars: 500 μm. **h**, The pimonidazole-positive area was quantified and normalized to total small intestine (SI) area ($n = 5$ mice per group). **i**, Wild-type mice treated with $H_2O$ or HFCS and total-body, constitutive *Glut5*$^{-/-}$ mice treated with HFCS were euthanized and intestines were fixed and examined by IHC. Representative images are shown. Scale bars, 200 μm (top); 50 μm (bottom). **j**, Wild-type mice treated with $H_2O$ or 25% HFCS ad libitum for four weeks were euthanized and intestinal epithelium was collected for western blot for indicators of cell health including markers of energy homeostasis (pACC, pAMPK) and anti-apoptotic proteins (BCL2, BCL-XL, MCL-1). **k**, Mice treated as in **j** were also euthanized and the intestinal epithelium was examined by western blot for hypoxia response proteins (ENO1, LDHA) and KHK. **b**, **c**, **e**, **h**, two-sided Student's *t*-test. NS, not significant; ***$P < 0.001$. All data are mean ± s.e.m. For gel source data, see Supplementary Fig. 1.

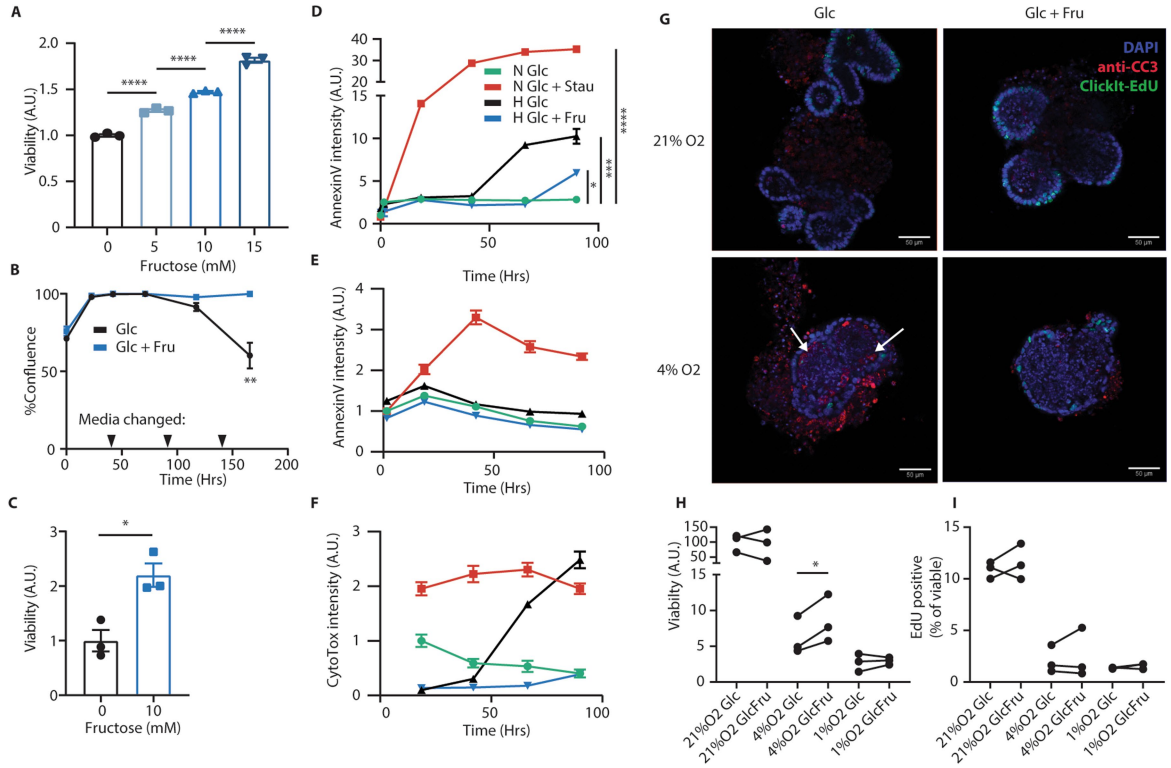


**Extended Data Fig. 4 | Fructose enhances hypoxic cell survival. a**, At the conclusion of the experiment depicted in Fig. 2a, HCT116 cells were collected and analysed by Trypan Blue exclusion assay. Total live cells per group were counted and normalized to the fructose-free group ($n = 3$ biological replicates per group). **b**, **c**, HCT116 cells were plated near confluence and cultured in hypoxia with or without 10 mM fructose in the medium. Every 48 h, as indicated, the medium was exchanged with fresh oxygen-equilibrated medium. Confluence was monitored and at the conclusion of the experiment cells were analysed by Trypan Blue exclusion assay as in **a** ($n = 3$ biological replicates per group). **d**–**f**, HCT116 (**d**) or DLD1 (**e**, **f**) cells were cultured with glucose and either stausporin (Stau, 100 nM, apoptotic control) or fructose, in medium that also contained an Annexin V dye (**d**, **e**) and a nucleic-acid-binding cell death dye (CytoTox; **f**). Cells were incubated in normoxia (N) or hypoxia (H) and imaged daily by live-cell imaging. Stain intensity is reported as positive cell area per well normalized to the initial normoxic glucose control ($n = 3$ biological replicates per data point). **g**, Intestinal organoids were generated from adult B6J mice and cultured in hypoxia with or without fructose for 72 h. At experiment termination, organoids were pulsed with EdU, fixed in situ, stained for the indicated targets and examined by confocal microscopy. Representative images are shown. White arrows indicate regions with intra-organoid CC3 puncti. Scale bars, 50 µm. **h**, **i**, Organoids treated as in **g** were rapidly dissociated and stained for viability (via a membrane-impermeable dye) (**h**) and EdU (**i**). The resulting cell suspensions were analysed by flow cytometry. Viability is expressed as viable cells recovered per culture well, normalized to the average of the normoxic glucose controls ($n = 3$ progenitor mice; each pair of points represents a different mouse progenitor). In these and other in vitro assays, unless otherwise noted, glucose was replenished daily as described in the Methods. **a**, **d**, **h**, One-way ANOVA followed by Holm–Sidak post-hoc test for multiple comparisons; **b**, **c**, two-sided Student's *t*-test; $^{*}P < 0.05$, $^{**}P < 0.01$, $^{****}P < 0.0001$. All data are mean ± s.e.m.

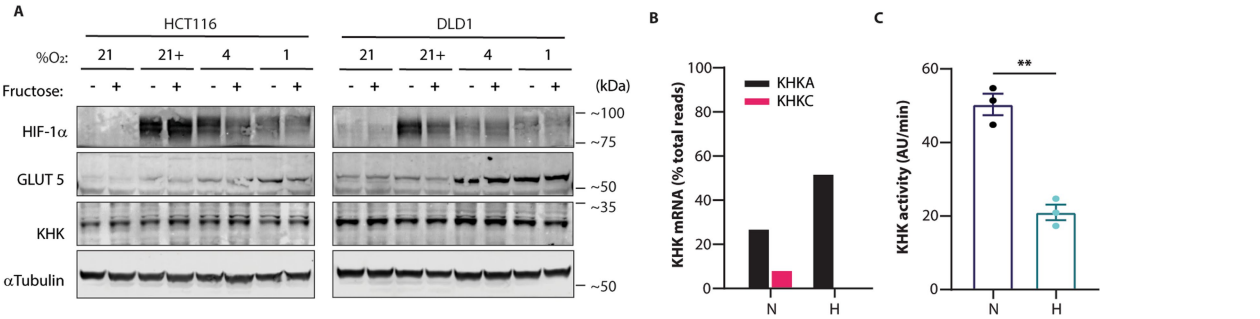


**Extended Data Fig. 5 | Hypoxia increases GLUT5 expression and KHK-A transcription. a**, HCT116 and DLD1 cells cultured at the indicated $O_2$ concentrations with or without 10 mM fructose were lysed at 36 h and western blotted for the indicated targets. '+' in the '%$O_2$' row indicates that 100 µM cobalt chloride was added to the medium at time 0. **b**, RNA was extracted from HCT116 cells treated in normoxia or hypoxia for 24 h and analysed by IsoSeq. The relative proportion of the A and C isoforms of KHK are shown ($n = 1$ biological replicate per $O_2$ condition). **c**, HCT116 cells cultured in normoxia or hypoxia for 24 h were lysed and tested for KHK activity by enzymatic assay ($n = 3$ biological replicates). **c**, Two-sided student's *t*-test. $^{**}P < 0.01$. Data in **c** are mean ± s.e.m. For gel source data, see Supplementary Fig. 1.

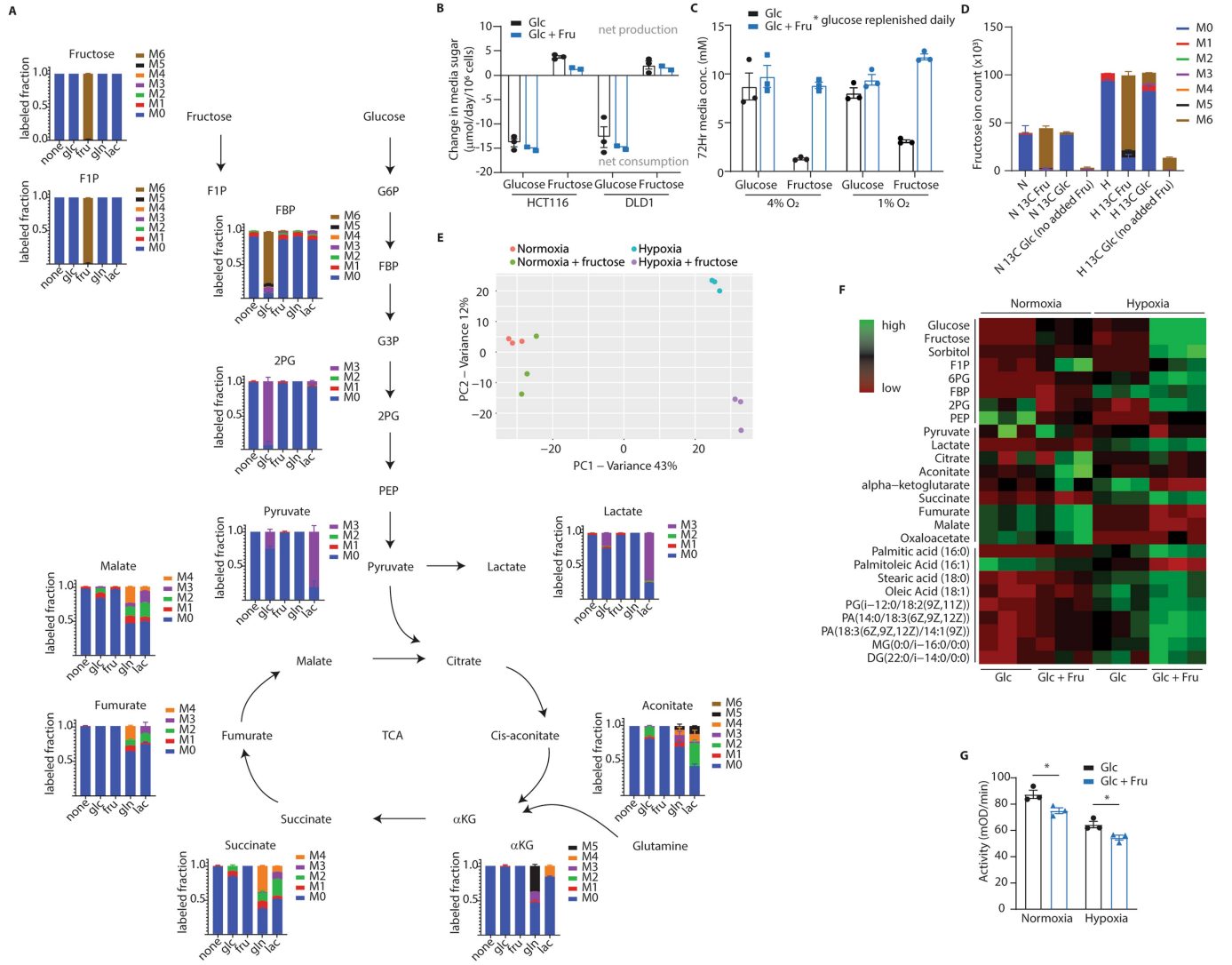


**Extended Data Fig. 6 | F1P accumulates in cells and correlates with marked metabolic changes in hypoxia. a**, HCT116 cells cultured in hypoxia with fructose were labelled with various U-$^{13}$C metabolites and intracellular metabolites were detected by LC–MS. The *y* axis reflects the fraction of the detected metabolite labelled with $^{13}$C on the number of carbons denoted by the colours to the right of each graph. The *x* axis denotes the labelled feed metabolite for that particular group. The graph for fructose, for example, indicates that all detected fructose ions were labelled at all 6 carbons with $^{13}$C when U-$^{13}$C6 fructose was provided in the medium ($n = 3$ biological replicates per unique label). **b**, HCT116 and DLD1 cells were cultured in hypoxia with 25 mM glucose with or without 10 mM fructose. At 48 h the growth medium was assayed for glucose and fructose content. Colours indicate the initial medium formulation for each group. The *x* axis denotes which sugar is being measured ($n = 3$ (Glc) and $n = 2$ (Glc + Fru) biological replicates per group). **c**, Mouse intestinal organoids were cultured in hypoxia with 10 mM glucose with or without 10 mM fructose for 72 h. Glucose in the 3-ml culture volume was increased by 5 mM daily to account for glucose depletion. After 72 h the growth medium was assayed for sugar content ($n = 3$ biological replicates per group, $n = 1$ from each progenitor mouse). **d**, HCT116 cells were treated with uniformly labelled $^{13}$C-fructose or glucose and isotopologues for intracellular fructose were generated. Unless otherwise noted, each column represents an experimental group that received some form of glucose and fructose ($n = 3$ biological replicates per *x*-axis label). N, normoxia; H, hypoxia). **e**, **f**, Principal component analysis (PCA) (**e**) targeted heat map (**f**) of metabolomics data from HCT116 cells cultured at confluence in hypoxia for 36 h and then collected for LC–MS. PCA data are centred and unit-variance-scaled; heat map data are row-normalized ion abundances ($n = 3$ biological replicates per group; loading plots available in Supplementary Fig. 3). **g**, Pyruvate kinase activity was measured by enzymatic assay in lysates from HCT116 cells cultured in normoxia or hypoxia for 24 h with or without fructose. Assay wells were loaded with equal amounts of total protein for each group ($n = 3$ biological replicates per group). G6P, glucose 6-phosphate; G3P, glyceraldehyde 3-phosphate; 2PG, 2-phosphoglycerate; TCA: tri-carboxylic acid cycle; αKG, α-ketoglutarate; PA: phosphatidic acid; MG: monoacylglycerol; DG: diacylglycerol. **g**, Two-way ANOVA followed by Holm–Sidak post-hoc test for multiple comparisons. $^*P < 0.05$. All error bars represent mean ± s.e.m.

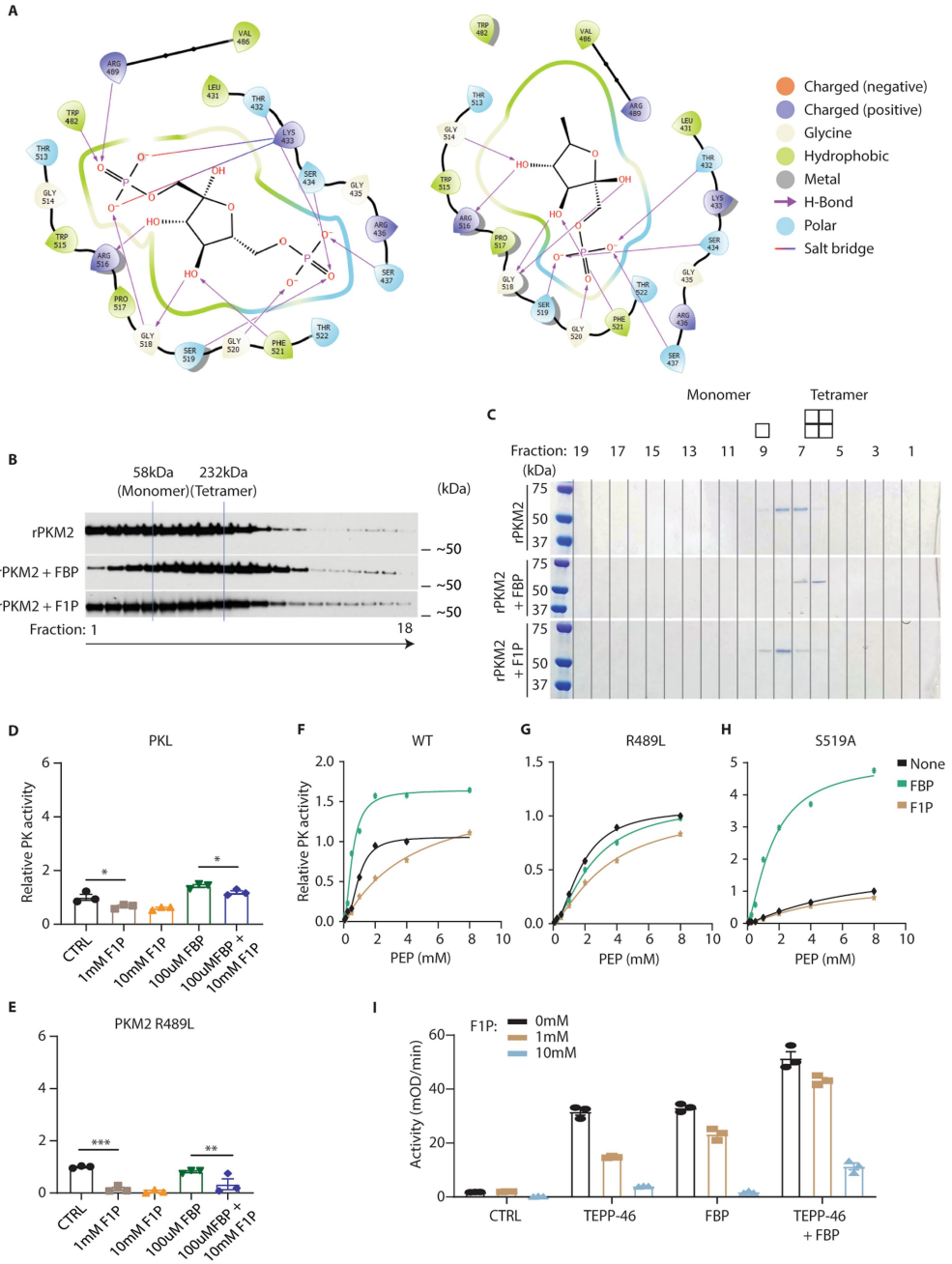


**Extended Data Fig. 7 | The FBP-binding pocket of PKM2 is important for F1P inhibition. a**, Simulated binding positions and residue interactions for FBP (left) and F1P (right) in the allosteric binding pocket of PKM2. Residues 482 and 489 are components of the FBP-activation loop that are predicted to interact with FBP but not F1P. **b**, Purified recombinant PKM2 (rPKM2) was incubated with the indicated metabolites and separated through a sucrose gradient (also containing the indicated metabolites). Fractions were removed from the gradients and analysed by SDS–PAGE and western blot for PKM2. FBP concentration, 100 μM; F1P concentration, 500 μM. **c**, Recombinant PKM2 incubated with the indicated metabolites was run on a gel filtration column and subjected to SDS–PAGE and Coomassie blue staining. FBP concentration during incubation and in the column, 100 μM; F1P concentration, 500 μM. **d**, **e**, The activity of recombinant PKL and the PKM2(R489L) mutant pre-incubated with the indicated metabolites was measured by enzymatic assay ($n = 3$ independent reaction wells per group). The residues responsible for PKM2 binding FBP are altered in these isoforms. **f**–**h**, Recombinant PKM2 mutants with alterations to the FBP-binding pocket were generated and assayed for PK activity with the indicated metabolites added at the incubation step. FBP concentration, 100 μM; F1P concentration, 1 mM ($n = 2$ wells per data point). **i**, The activity of recombinant PK pre-incubated concurrently with the indicated metabolites or compounds was measured by enzymatic assay ($n = 3$ wells per group). **d**, **e**, One-way ANOVA followed by Holm–Sidak post-hoc test for multiple comparisons. $^{*}P < 0.05$, $^{**}P < 0.01$, $^{***}P < 0.001$. Error bars represent mean ± s.e.m. For gel source data, see Supplementary Fig. 1.

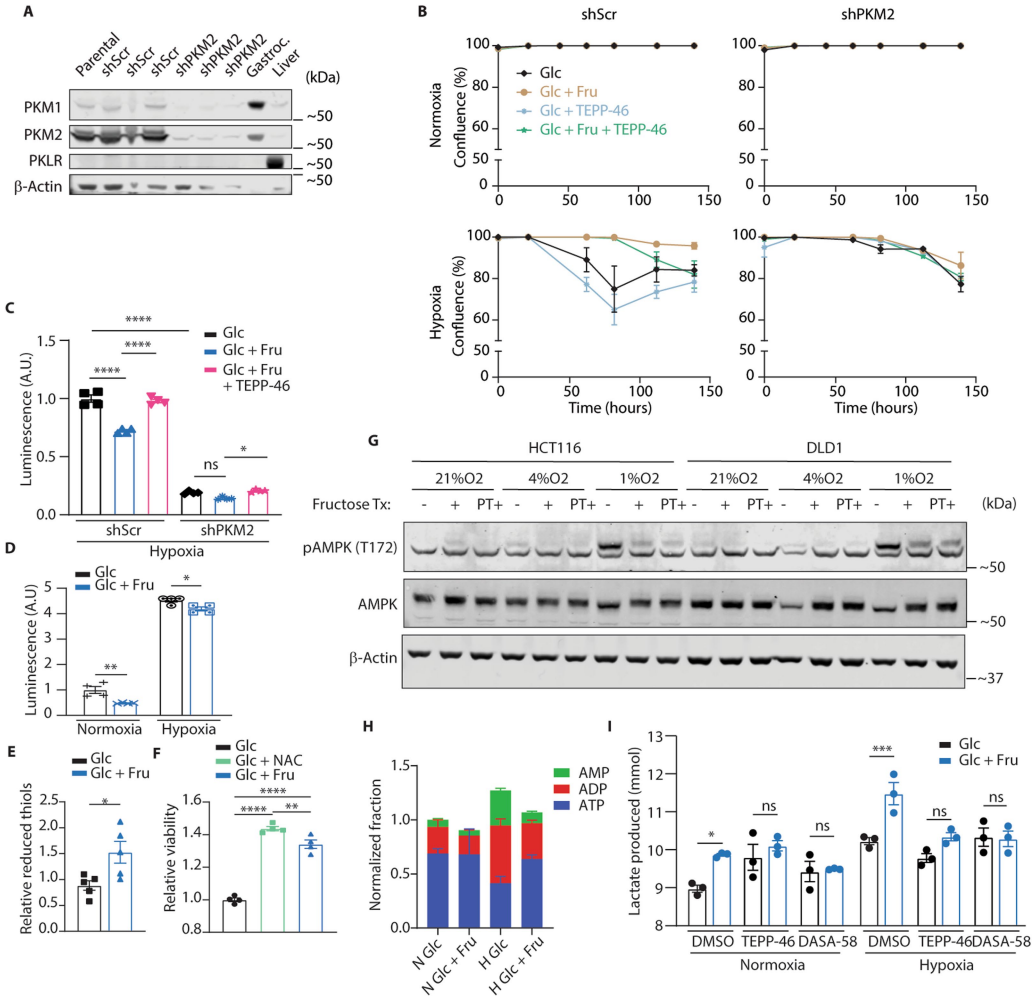


**Extended Data Fig. 8 | Fructose and pyruvate kinase activation modulate cell survival in hypoxia. a**, HCT116 cells were transduced with shRNA targeting a scrambled sequence (shScr) or PKM2 (sh*PKM2*). Two weeks after transduction, parental cells as well as these modified lines were western blotted for the protein targets indicated on the left. Three separate shScr and sh*PKM2* subclones were analysed. Mouse gastrocnemius (gastroc.) muscle and liver tissue were used as PKM1 and PKLR controls, respectively. β-actin was used as a loading control. **b**, HCT116 cells expressing the indicated shRNAs were cultured in normoxia or hypoxia with or without fructose and TEPP-46 (50 μM) in the medium. Glucose was replenished daily, and confluence was monitored by live-cell imaging ($n = 3$ biological replicates per group). **c**, shScr or sh*PKM2*-transduced HCT116 cells were cultured in hypoxia for 24 h with or without fructose or fructose and TEPP-46 (50 μM). Total cell $H_2O_2$ was then measured using a luciferase-based assay ($n = 4$ biological replicates per group). **d**, Parental HCT116 cells were subjected to the same treatment as in **c**, but were cultured for 72 h in normoxia or hypoxia with daily glucose replenishment ($n = 4$ biological replicates per group). **e**, HCT116 cells cultured in hypoxia for 24 h were assayed for reduced thiols ($n = 5$ biological replicates per group). **f**, HCT116 cells cultured in hypoxia were provided with 10 mM glucose, 10 mM glucose with *N*-acetylcysteine (NAC) or 5 mM glucose and 5 mM fructose in the medium. After 144 h the viability of the adherent cells was measured ($n = 4$ biological replicates per group). **g**, HCT116 and DLD1 cells were subjected to varying levels of hypoxia for 24 h with fructose introduced in the medium either at the time the cells were placed in hypoxia ('+') or as pre-treatment ('PT+'), starting in the previous cell passage before plating the experiment and continuing through the hypoxic period (4 days total fructose exposure with the final 24 h in hypoxia). Cells were rapidly lysed at the conclusion of the experiment and analysed by western blot. **h**, HCT116 cells were exposed to hypoxia with or without fructose in the medium and LC–MS analysis was performed on the resulting polar extracts ($n = 3$ biological replicates per group). **i**, HCT116 cells were cultured in normoxia or hypoxia for 24 h with or without fructose. At the end of the experiment, medium samples were taken from each well and analysed by enzymatic assay for lactate content ($n = 3$ biological replicates per group). **c**, **d**, **i**, Two-way ANOVA followed by Holm–Sidak post-hoc test for multiple comparisons; **e**, Student's two-sided *t*-test; **f**, one-way ANOVA followed by Holm–Sidak post-hoc test for multiple comparisons. NS, not significant; $^*P < 0.05$, $^{**}P < 0.01$, $^{***}P < 0.001$, $^{****}P < 0.0001$. All data are mean ± s.e.m. where possible. For gel source data, see Supplementary Fig. 2.

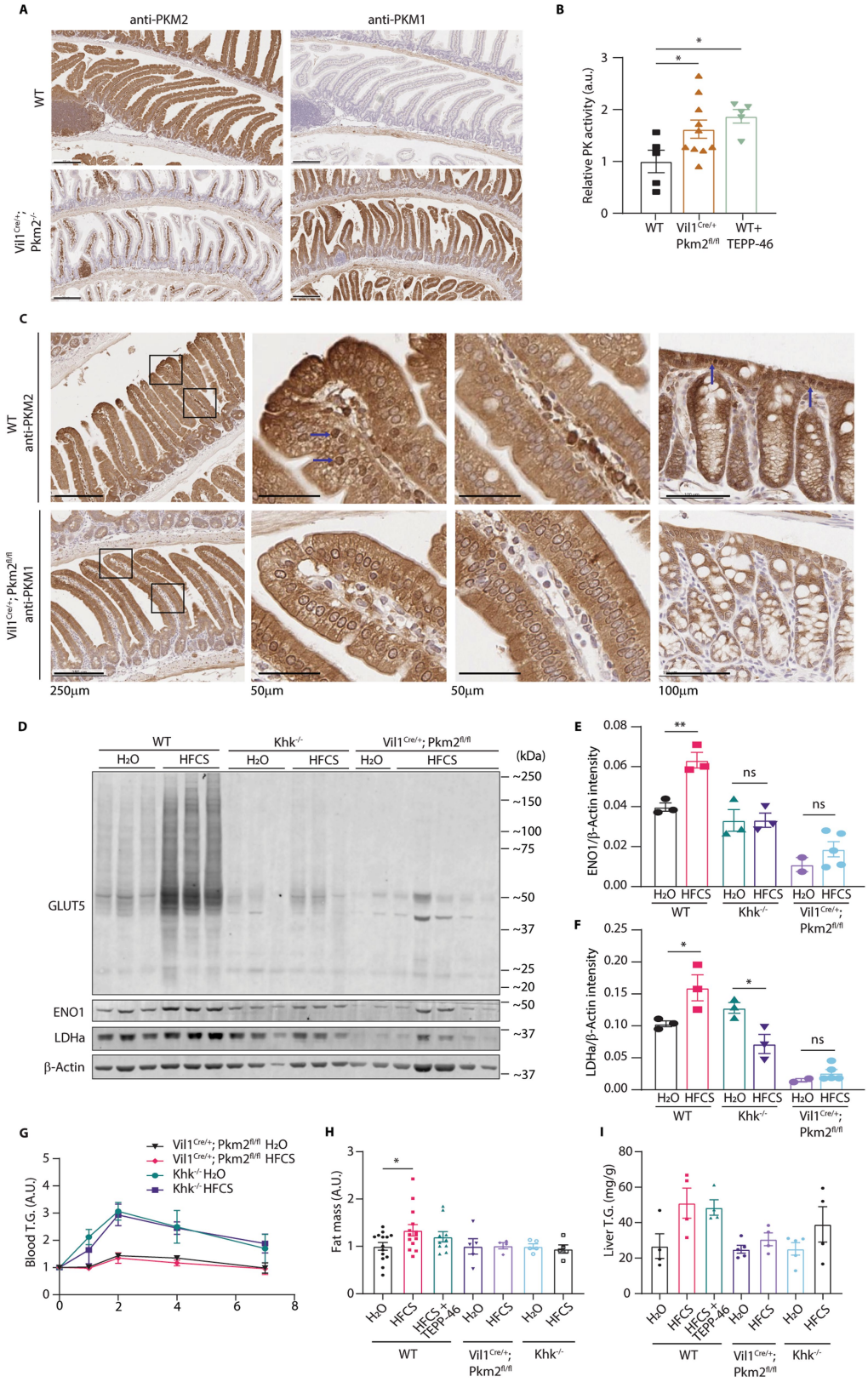


**Extended Data Fig. 9** | See next page for caption.

**Extended Data Fig. 9 | Ablation of PKM2 in the villi results in upregulation of PKM1. a**, Representative intestines from 12-week-old mice examined by IHC for the indicated targets. Scale bar, 200 μm. **b**, Mouse IEC lysates from wild-type mice, *Vil1*$^{Cre/+}$;*Pkm2*$^{f/f}$ mice and wild-type mice treated with TEPP-46 were analysed by enzymatic assay for pyruvate kinase activity (mice per group: left to right: 5, 10, 5). Same final protein concentration in each reaction well. **c**, Wild-type and *Vil1*$^{Cre/+}$;*Pkm2*$^{f/f}$ mice were euthanized and intestines were fixed and examined by IHC against PKM2 or PKM1, respectively. The left column shows proximal jejunum villi in each mouse, and the next two columns are high-magnification images of the distal and proximal villus in each mouse. The last column is colon epithelium. Blue arrows indicate nuclei with intense staining. Scale bars for each row are as indicated. **d**, Wild-type, *Khk*$^{-/-}$ and *Vil1*$^{Cre/+}$;*Pkm2*$^{f/f}$ mice were treated with $H_2O$ or HFCS and the intestinal epithelium was examined by western blot. **e**, **f**, LDHA and ENO1 intensity were quantified relative to the β-actin loading control (mice per group: left to right: 3, 3, 3, 3, 2, 5). **g**, Serum triglyceride (T.G.) after a lipid challenge was measured in mice fed $H_2O$ or 25% HFCS by daily oral gavage for two weeks. Units are normalized to the initial time point to highlight changes in blood triglyceride after the bolus (mice per group; top to bottom: 7, 6, 5, 5). **h**, After two weeks on the diet mice were euthanized, and the gonadal fat deposits were weighed. Units represent total gonadal depot fat mass as a percentage of total body mass, normalized to $H_2O$-treated mice (mice per group: left to right: 14, 14, 10, 5, 4, 5, 5). **i**, Liver was also collected and analysed for triglyceride content per gram of tissue (mice per group: left to right: 4, 4, 4, 5, 4, 5, 4). **b**, **h**, One-way ANOVA followed by Holm–Sidak post-hoc test for multiple comparisons; **e**, **f**, two-way ANOVA followed by Holm–Sidak post-hoc test for multiple comparisons. NS, not significant; $^{*}P < 0.05$, $^{**}P < 0.01$; all data are mean ± s.e.m. For gel source data, see Supplementary Fig. 2.

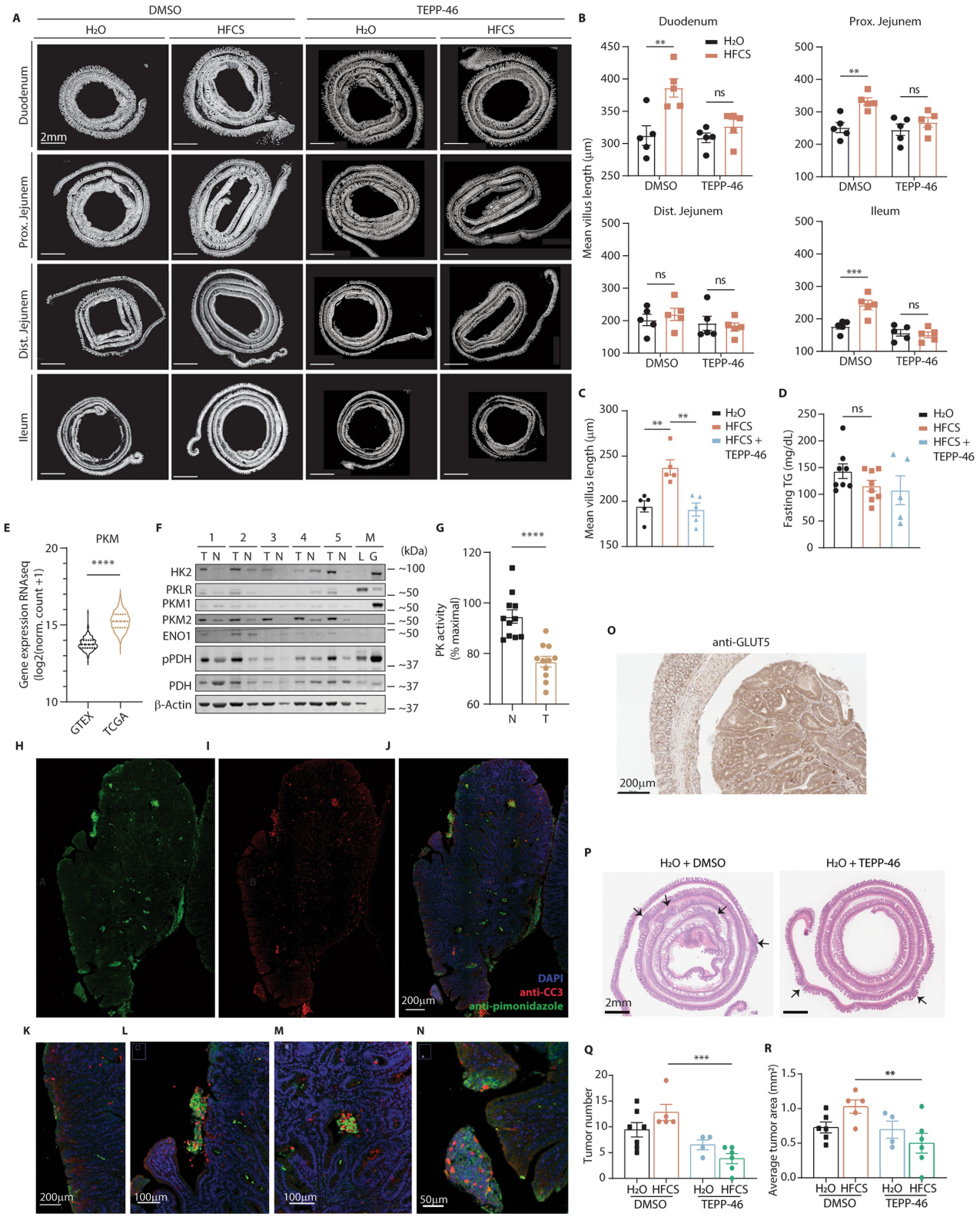


**Extended Data Fig. 10** | See next page for caption.

**Extended Data Fig. 10 | TEPP-46 ablates HFCS-induced villus elongation and tumour growth. a**, Wild-type mice provided with a daily oral gavage of HFCS or $H_2O$ mixed with DMSO or TEPP-46 were euthanized after 10 days. Intestines were collected and analysed for mean villus length. **b**, Villi measurements for those same sections ($n = 5$ mice per group). **c**, Mice were treated with normal chow and water for two weeks, 25% HFCS by daily gavage for two weeks or HFCS for two weeks followed by HFCS with TEPP-46 (2 mg per kg per day) for another two weeks. At the conclusion of these treatments, the mice were euthanized and small intestine villus length was examined ($n = 5$ mice per group). **d**, Mice were fed the indicated diets by oral gavage for two weeks and serum triglyceride content was measured during the fasted state (mice per group: left to right: 8, 8, 5). **e**, Violin plot of gene expression data from GTEX (normal human colon epithelium) and TCGA (human colon adenocarcinoma) are shown for PKM. **f**, Samples of colon tumour (T) and matched normal epithelium (N) from patients with CRC were lysed and analysed by western blot for pyruvate kinase isoform expression and hypoxia markers. Mouse liver and gastrocnemius are included as controls. **g**, Pyruvate kinase activity was measured in lysates from patient samples before and after incubation with PK activator, and the ratio of initial versus activated activity is shown (tumour and adjacent normal tissue pairs from $n = 11$ individuals). **h**–**j**, Single channels and composite image of normal-diet-treated $Apc^{Q1405X/+}$ intestinal tumours stained with DAPI, anti-CC3 and anti-pimonidazole and examined by immunofluorescence. **k**–**n**, Fly-out panels depicting areas of CC3 and pimonidazole colocalization both along the tumour periphery (**k**, **l**) and in the tumour core (**m**, **n**). Scale bars as indicated. **o**, Normal-diet-treated intestinal tumours were also examined by IHC using anti-GLUT5. Scale bar, 200 µm. **p**, Representative H&E-stained Swiss-rolled intestines from $APC^{Q1405X/+}$ mice treated with the indicated regimens. Arrows indicate tumours. Scale bars, 2 mm. **q**, **r**, H&E images of Swiss-rolled intestines were analysed for tumour burden. Each tumour in the section was counted and its cross-sectional area measured (mice per group: left to right: 6, 5, 4, 6). **b**, **q**, **r**, Two-way ANOVA followed by Holm–Sidak post-hoc test for multiple comparisons; **c**, **d**, one-way ANOVA followed by Holm–Sidak post-hoc test for multiple comparisons; **e**, **g**, two-sided Student's *t*-test. NS, not significant; $^{**}P < 0.01$, $^{***}P < 0.001$, $^{****}P < 0.0001$. All error bars represent mean ± s.e.m. For gel source data, see Supplementary Fig. 2.

nature research

Corresponding author(s): Marcus D. Goncalves

Last updated by author(s): Jun 16, 2021

# Reporting Summary

Nature Research wishes to improve the reproducibility of the work that we publish. This form provides structure for consistency and transparency in reporting. For further information on Nature Research policies, see Authors & Referees and the Editorial Policy Checklist.

## Statistics

For all statistical analyses, confirm that the following items are present in the figure legend, table legend, main text, or Methods section.

| n/a | Confirmed | |
|---|---|---|
| ☐ | ☒ | The exact sample size (*n*) for each experimental group/condition, given as a discrete number and unit of measurement |
| ☐ | ☒ | A statement on whether measurements were taken from distinct samples or whether the same sample was measured repeatedly |
| ☐ | ☒ | The statistical test(s) used AND whether they are one- or two-sided<br>*Only common tests should be described solely by name; describe more complex techniques in the Methods section.* |
| ☒ | ☐ | A description of all covariates tested |
| ☐ | ☒ | A description of any assumptions or corrections, such as tests of normality and adjustment for multiple comparisons |
| ☐ | ☒ | A full description of the statistical parameters including central tendency (e.g. means) or other basic estimates (e.g. regression coefficient) AND variation (e.g. standard deviation) or associated estimates of uncertainty (e.g. confidence intervals) |
| ☐ | ☒ | For null hypothesis testing, the test statistic (e.g. *F*, *t*, *r*) with confidence intervals, effect sizes, degrees of freedom and *P* value noted<br>*Give P values as exact values whenever suitable.* |
| ☒ | ☐ | For Bayesian analysis, information on the choice of priors and Markov chain Monte Carlo settings |
| ☒ | ☐ | For hierarchical and complex designs, identification of the appropriate level for tests and full reporting of outcomes |
| ☒ | ☐ | Estimates of effect sizes (e.g. Cohen's *d*, Pearson's *r*), indicating how they were calculated |

*Our web collection on statistics for biologists contains articles on many of the points above.*

## Software and code

Policy information about availability of computer code

| | |
|---|---|
| Data collection | *Provide a description of all commercial, open source and custom code used to collect the data in this study, specifying the version used OR state that no software was used.* |
| Data analysis | Aperio ImageScope 12.4, Fiji, MATLAB R2019b, XCMS Online 3.7.1, X13CMS |

For manuscripts utilizing custom algorithms or software that are central to the research but not yet described in published literature, software must be made available to editors/reviewers. We strongly encourage code deposition in a community repository (e.g. GitHub). See the Nature Research guidelines for submitting code & software for further information.

## Data

Policy information about availability of data

All manuscripts must include a data availability statement. This statement should provide the following information, where applicable:

- Accession codes, unique identifiers, or web links for publicly available datasets
- A list of figures that have associated raw data
- A description of any restrictions on data availability

All figures include associated raw data. Additional data that support the findings of this study are available from the corresponding author upon reasonable request.

# Field-specific reporting

Please select the one below that is the best fit for your research. If you are not sure, read the appropriate sections before making your selection.

☒ Life sciences ☐ Behavioural & social sciences ☐ Ecological, evolutionary & environmental sciences

# Life sciences study design

All studies must disclose on these points even when the disclosure is negative.

| | |
|---|---|
| Sample size | Sample sizes were determined in accordance with the literature and based on previous experience in our group. |
| Data exclusions | APC1405 animals used for breeding purposes were excluded from the trial. |
| Replication | Experimental findings were verified by using multiple mice or culture vessels in each study as replicates. Replications were successful. |
| Randomization | Mice of different genotypes were randomly assigned to treatment groups throughout this study. |
| Blinding | Villus length measurement was performed in a blinded manner via an automated image analysis program. Sample preparation and data acquisition for metabolomics were performed in a blinded manner. Tumor quantification was performed in a blinded manner. |

# Reporting for specific materials, systems and methods

We require information from authors about some types of materials, experimental systems and methods used in many studies. Here, indicate whether each material, system or method listed is relevant to your study. If you are not sure if a list item applies to your research, read the appropriate section before selecting a response.

## Materials & experimental systems

| n/a | Involved in the study |
|---|---|
| ☐ | ☒ Antibodies |
| ☐ | ☒ Eukaryotic cell lines |
| ☒ | ☐ Palaeontology |
| ☐ | ☒ Animals and other organisms |
| ☒ | ☐ Human research participants |
| ☒ | ☐ Clinical data |

## Methods

| n/a | Involved in the study |
|---|---|
| ☒ | ☐ ChIP-seq |
| ☐ | ☒ Flow cytometry |
| ☒ | ☐ MRI-based neuroimaging |

## Antibodies

| | |
|---|---|
| Antibodies used | PKM1 (CST, Cat. #7067), GLUT5 (Santa Cruz Biotechnology, Cat. #271055), PKM2 (CST, Cat. #4053), β-actin (Abcam, Cat. #6276), Hif1a (CST, Cat. #36169), a-tubulin (CST, Cat. #3873), cleaved caspase-3 (CST, Cat. #9661), KHK (Abcam, Cat. #ab154405), PKL (Abcam, Cat. #ab171744), BrdU (mouse, Santa Cruz Biotechnology (SC) Cat. # sc-32323), and Pimonidazole-adducts (mouse, Hypoxyprobe Inc. Cat # Mouse-Mab). All antibodies were used at the manufacturer's recommended dilution.<br><br>A complete list of all antibodies used as well as dilutions used is included in the methods. |
| Validation | All antibodies were used in accordance to the manufacturer guidelines and confirmed to have previously been documented in the literature through CiteAb (www.citeab.com). |

## Eukaryotic cell lines

Policy information about cell lines

| | |
|---|---|
| Cell line source(s) | All cell lines were procured from ATCC. |
| Authentication | All cell lines were verified by ATCC sequencing. |
| Mycoplasma contamination | All cell lines were confirmed to be uncontaminated. |
| Commonly misidentified lines (See ICLAC register) | *Name any commonly misidentified cell lines used in the study and provide a rationale for their use.* |

## Animals and other organisms

Policy information about studies involving animals; ARRIVE guidelines recommended for reporting animal research

| | |
|---|---|
| Laboratory animals | 6-8 week old male and female C57B6/J, C57B6/NJ, FVB, and BALBC mice were obtained from The Jackson Laboratory. Mixed-background male and female "G5H" mice were kindly shared by Andrew Dannenberg. Vil1Cre/+; PKM2fl/fl mice were generated from crossing B6.Cg-Tg(Vil1Cre/+)997Gum/J (stock # 004586) and B6;129S-Pkmtm1.1Mgvh/J (stock # 024048) mice purchased from The Jackson Laboratory. KHK-/-mice lacking both KHK-A and KHK-C on the C57BL/6 background were kindly shared by Dr. |

| | |
|---|---|
| | Bonthron at University of Leeds at UK and Drs. Lanaspa and Johnson at University of Colorado. APCQ1405X/+ ("APC1405") mice on the C57BL/6N background were kindly shared by Dr. Lukas Dow at Weill Cornell Medical College. |
| Wild animals | *Provide details on animals observed in or captured in the field; report species, sex and age where possible. Describe how animals were caught and transported and what happened to captive animals after the study (if killed, explain why and describe method; if released, say where and when) OR state that the study did not involve wild animals.* |
| Field-collected samples | *For laboratory work with field-collected samples, describe all relevant parameters such as housing, maintenance, temperature, photoperiod and end-of-experiment protocol OR state that the study did not involve samples collected from the field.* |
| Ethics oversight | All animal studies were approved by the Institutional Animal Care and Use Committee (IACUC) of Weill Cornell Medical College and maintained as approved by the Institutional Animal Care and Use Committee (IACUC) at Weill Cornell Medicine (NY) under protocol number 2012-0074. |

Note that full information on the approval of the study protocol must also be provided in the manuscript.

# Flow Cytometry

## Plots

Confirm that:

☒ The axis labels state the marker and fluorochrome used (e.g. CD4-FITC).

☒ The axis scales are clearly visible. Include numbers along axes only for bottom left plot of group (a 'group' is an analysis of identical markers).

☒ All plots are contour plots with outliers or pseudocolor plots.

☒ A numerical value for number of cells or percentage (with statistics) is provided.

## Methodology

| | |
|---|---|
| Sample preparation | Organoid EdU flow cytometry was performed using the ClickiT Plus EdU Alexa Fluor 647 Flow Cytometry Assay Kit (Thermo Fisher Scientific, # C10634). Each well of a 6-well plate was broken up by pipetting vigorously 50 times in 1 mL PBS, then diluted in 5 mL of PBS. Cells were pelleted at 1,100 rpm × 4 minutes at 4°C, then resuspended in 50 µL TrypLE and incubated at 37°C for 5 minutes. Five milliliters of PBS was then added to inactivate the TrypLE, and cells were pelleted. Cells were resuspended in 250 µL of 1% BSA in PBS, transferred to a 1.7-mL tube, and then pelleted at 3,000 rpm × 4 minutes. Cells were then stained with Live/dead fixable green viability dye (ThermoFisher, L34969) per the manufacturer's instructions. Cells were then resuspended in 100 µL Click-iT fixative, and processed as instructed in the Click-iT Plus EdU protocol (starting with Step 4.3). Wash and reaction volumes were 250 µL. Upon completion of staining, all cells from each well were resuspended in 250 µL 1% BSA in PBS and 200 µL of this suspension was analyzed using an Attune NxT flow cytometer (ThermoFisher). Viable and proliferating cells were identified by the gating strategy depicted in Fig. S26. |
| Instrument | Attune NXT |
| Software | FlowJo |
| Cell population abundance | The abundance of the final populations ranged from 5000 to 50000 events. |
| Gating strategy | The gating strategy is shown in Fig. S26 |

☒ Tick this box to confirm that a figure exemplifying the gating strategy is provided in the Supplementary Information.